MICROCOPY RESOLUTION TEST CHART
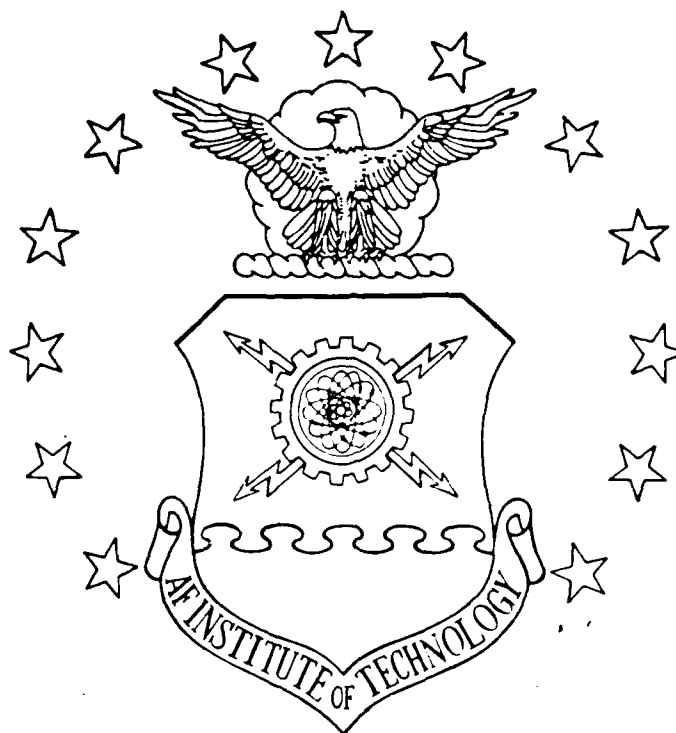
NATIONAL BUREAU OF STANDARDS-1963

①

AD-A189 630

CALCULATING DEPLETION REGION CARRIER
CONCENTRATIONS WITH CAPACITANCE-VOLTAGE
MEASUREMENTS AND ETCHING

THESIS

Gordon H. Gainer, Jr.
Captain, USAF

AFIT/GEP/ENP/87D-8

DTIC
ELECTE
MAR 03 1988
S
E
D

DEPARTMENT OF THE AIR FORCE

AIR UNIVERSITY

# AIR FORCE INSTITUTE OF TECHNOLOGY

Wright-Patterson Air Force Base, Ohio

88 3 01 043

CALCULATING DEPLETION REGION CARRIER
CONCENTRATIONS WITH CAPACITANCE-VOLTAGE
MEASUREMENTS AND ETCHING

THESIS

Gordon H. Gainer, Jr.
Captain, USAF

AFIT/GEP/ENP/87D-8

CALCULATING DEPLETION REGION CARRIER CONCENTRATIONS WITH
CAPACITANCE-VOLTAGE MEASUREMENTS AND ETCHING

THESIS

Presented to the Faculty of the School of Engineering

of the Air Force Institute of Technology

Air University

In Partial Fulfillment of the

Requirements for the Degree of

Masters of Science in Engineering Physics

Gordon H. Gainer, Jr., B.S.

Captain, USAF

December 1987

Approved for Public Release; Distribution Unlimited

## Preface

The purpose of this study was to find a method of measuring the concentrations of charge carriers in n-type semiconductors within the initial depletion region. This method was to use capacitance-voltage measurements and the etching of layers from the semiconductor surface. All the necessary lab work was carried out at the Avionics Laboratory.

I wish to express great appreciation to several people of the Avionics Laboratory who helped me a great deal, such as Lt David Elsaesser, Capt Michael Sopko, Ben Carroll, Robert Neidhard, Michael Curtis, Mary Harshbarger, and Sgt James Foster. I wish also to express thanks to Dr. Y.K. Yeo, my thesis chairman.

Gordon H. Gainer, Jr.

# Table of Contents

## List of Figures

## Abstract

Methods were developed for finding the charge carrier

concentrations within the initial depletion region of n-type

semiconductors. These methods combine the capacitance-

voltage (C-V) technique with the etching of layers from the

semiconductor surface. After each etch, the depletion

region is made to end at the same location within the

semiconductor. This location is used as a common reference

and is arbitrarily chosen at a distance deep below the

original unetched surface. For each etch depth, the voltage

which extends the depletion region to the common reference

distance is found. The voltage drop from an etch depth to

the deeper common reference distance is the same as it would

be if the semiconductor was not etched. This voltage drop

is the sum of the applied voltage and the built-in

potential. The built-in potential depends on the barrier

potential at the semiconductor surface and the concentration

at the common reference distance. Assuming the barrier

potential is the same for each etch surface, the built-in

potential is constant for each etch. Consequently, the

applied bias voltage at each etch surface, can be treated as

the potential at that etch depth. Then equations, such as

Poisson's equation, can be used to find the carrier

concentrations within the initial depletion region. These

methods were successfully applied to ideal computer

generated C-V data as well as experimental C-V measurements of
Si-implanted GaAs.

# CALCULATING DEPLETION REGION CARRIER CONCENTRATIONS WITH CAPACITANCE-VOLTAGE MEASUREMENTS AND ETCHING

## I. Introduction

Ion implantation of semiconductors is widely used in fabricating electronic and opto-electronic devices, such as FETs (field effect transistors), ICs (integrated circuits), and laser diodes. Si-implanted GaAs is widely used because of its high electron mobility and high electrical activation efficiency. Ion implantation gives higher precision and control of dopant profiles in semiconductors than epitaxial growth or thermal diffusion. Theoretically, a continuous variation of the fluence and energy of the incident ions can produce any desired dopant distribution (1:9). In addition, ion implantation can produce good uniformity of implants over large regions, as well as reproducibility from wafer to wafer (2:122). The electronic and opto-electronic device performances depend strongly upon the charge carrier depth profiles. For example, active layers in microwave FETs must be precisely controlled to depths of about 1 micron (3:14). Therefore, it is very important to be able to accurately measure the carrier profiles. These carrier profiles are usually obtained by the capacitance-voltage (C-V) method or by Hall-effect measurements. However, both methods have different advantages and limitations.

1

The differential Hall method can be used for both n- and p-type materials, but it is destructive. In this method, a Hall-effect measurement is made of the sheet carrier concentration, the electrically active carriers below the semiconductor surface per unit surface area. Then a thin layer is removed by chemical etching. Another Hall-effect measurement of the sheet carrier concentration can be used to find the carrier concentration in the removed layer. A problem not usually taken into account in differential Hall profiling is that a surface depletion region, produced by the filling of acceptor-type surface electronic states, causes the measured profile to be shifted from the true profile and contracted. However, a surface depletion correction can be made to the measured apparent Hall profiles (4:5070-5075).

The C-V method uses a reversed biased Shottky barrier on the semiconductor to create a variable depletion width, which can be found from its capacitance. The density of carriers at the edge of the depletion width can be found from the differential change of capacitance with bias voltage. The C-V method is nondestructive. However, the C-V method does not give a profile within the initial depletion width at zero bias voltage, and this depletion width often is 0.2 $\mu$m. Also, the C-V method can be practically applied only to n-type materials.

## Thesis Objective and Scope

The objective of this thesis was to develop a method of calculating the carrier concentrations within the initial depletion region of semiconductors by combining C-V measurements with etching. The method was to be tested on Si-implanted GaAs. The GaAs samples used were <100> oriented and usually Cr-doped during crystal growth. The samples had been ion implanted at room temperature at an ion energy of 100 or 200 keV. The ion dose was $8 \times 10^{12}$ or $1 \times 10^{13}$ $cm^{-2}$. The samples were annealed at 800 or 850 °C for 15 minutes.

## Sequence of Presentation

Chapter II provides background information on ion implantation and ion range statistics. Chapter II also reviews the theoretical basis of the C-V method and the cause of the initial depletion region. Chapter III describes the Si-implanted GaAs sample preparation and C-V measurements. Chapter IV discusses the theory of the methods developed for finding the depletion region concentrations, starting with Poisson's equation. Chapter V describes the computer programs developed to analyze and implement the methods. Chapter VI shows and discusses the performance of the methods. Chapter VII presents the successful conclusions of this study and the recommendations for further study.

## II. Background

### Ion Implantation

The electrical and optical properties of a semiconductor material can be altered by doping -- adding impurities. The impurities can be added before the semiconductor crystallizes from the liquid state or by diffusion or ion implantation afterwards. Chromium is often added during crystal growth to electrically compensate for other trace impurities. Thermal diffusion is used for uniform doping over large crystal sections. In ion implantation, the dopants penetrate into the semiconductor as an energetic ion beam. Ion implantation has the advantages of a wide choice of dopants, high accuracy in the dopant concentration and area of doping, a well defined dopant profile, slight lateral spreading, good reproducibility, and high yields at low cost. Ion implantation can also be used at low temperatures, and it can have good uniformity over large areas.

The ion bombardment has the disadvantage of causing radiation damage, such as vacancies, interstitials, clusters of point defects, dislocations and dislocation loops, and stacking faults, within the crystal structure. Also, some of the implanted ions do not go into substitutional lattice sites to become electrically active. These problems can be mostly corrected by annealing the crystal. At the high

annealing temperatures (800 - 1000 °C), dopant and substrate atoms can diffuse out of the crystal. This is prevented by encapsulating the crystal surface before annealing.

Lindhard, Sharff, and Schiott (LSS) Theory

In ion implantation, the dopant ions suffer collisions with the substrate nuclei and electrons before stopping. The LSS theory takes into account the electronic and nuclear stopping powers to calculate the penetration depth. The penetration depth depends on the initial kinetic energy of the incident ion, the atomic number and atomic mass of the incident ion and substrate atoms, the temperature, etc. Lindhard, Sharff, and Schiott used the Thomas-Fermi interatomic potential to calculate the ion energy loss due to nuclear collisions and the range or depth that ions would go below the surface of the substrate. Assuming a Gaussian range distribution, they also calculated a mean square fluctuation in this range (1:36-39). The ion implanted dopant concentration is then given by

$$N(x_p) = \frac{\phi}{\sigma_p \sqrt{2\pi}} \ EXP\left[\frac{-(x_p - R_p)^2}{2\sigma_p^2}\right] \qquad (2.1)$$

where $N(x_p)$ is the dopant concentration at a depth $x_p$ measured along the ion beam direction, $\phi$ is the ion beam fluence, and $\sigma_p$ is the standard deviation in the projected range $R_p$. This is illustrated in Figure 1. Gibbons et al (5) developed a computer program to calculate the range and standard deviation for various implanted ions and

5
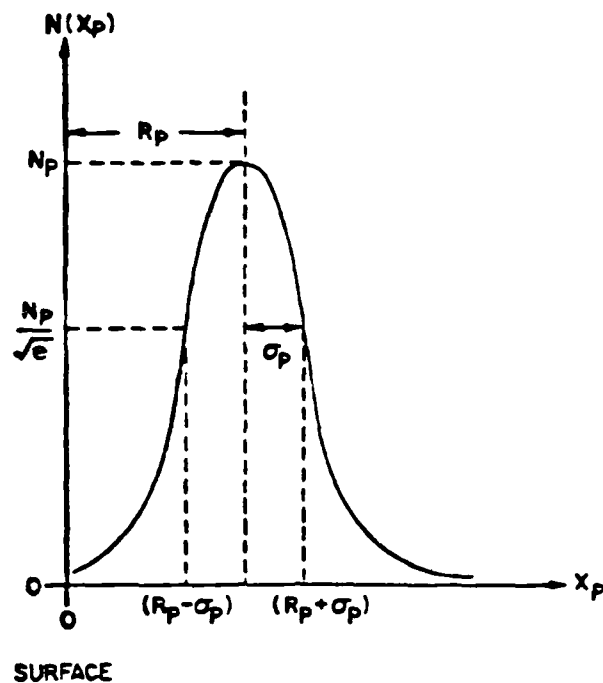
Figure 1.   LSS Theoretical Ion Depth Profile

substrates.   For example, Si ions with an energy of 100 keV
have a projected range in GaAs of 0.085 $\mu$m and a standard
deviation of 0.0442 $\mu$m.

The Gaussian distribution is for the random collisions
within an amorphous solid.   However, in a crystal, the ions
can be channeled down a major crystal axis and penetrate to
much greater depths than in an amorphous solid.   This
channeling is prevented by aligning the ion beam at an angle
to the major crystal axis, as shown in Figure 2 (6:13).
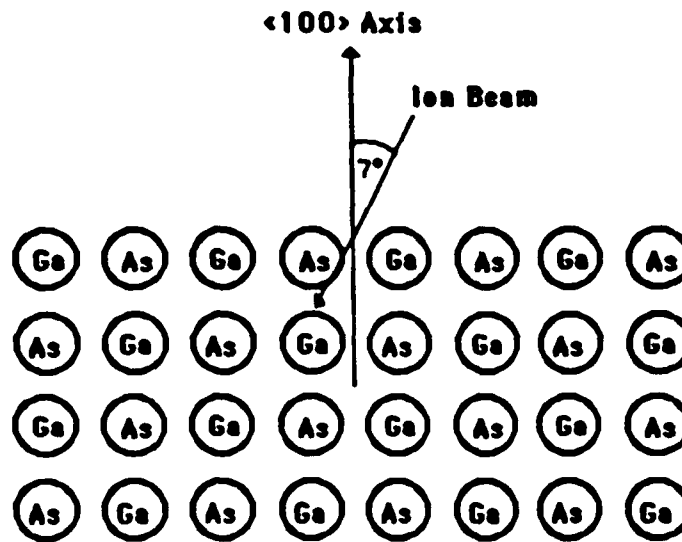
Figure 2.  Ion Beam Orientation to Prevent Channelin

## Depletion Region of Metal-Semiconductor Contacts

When a metal is brought into contact with an n-type
semiconductor, the Fermi energy level $E_F$ stays constant
across the metal-semiconductor boundary as shown in the
energy-band diagram of Figure 3.  The conduction band
minimum $E_C$ of the semiconductor starts out level at a
distance W from the metal and then rises to a barrier height
$q\phi_B$ at the metal surface, where q is the electronic charge
and $\phi_B$ is the barrier potential.  The built-in potential $V_{bi}$
is the difference between the potential at the metal surface
and the potential at W.  This built-in potential transfers
electrons to the metal and ionizes donor atoms from the

7
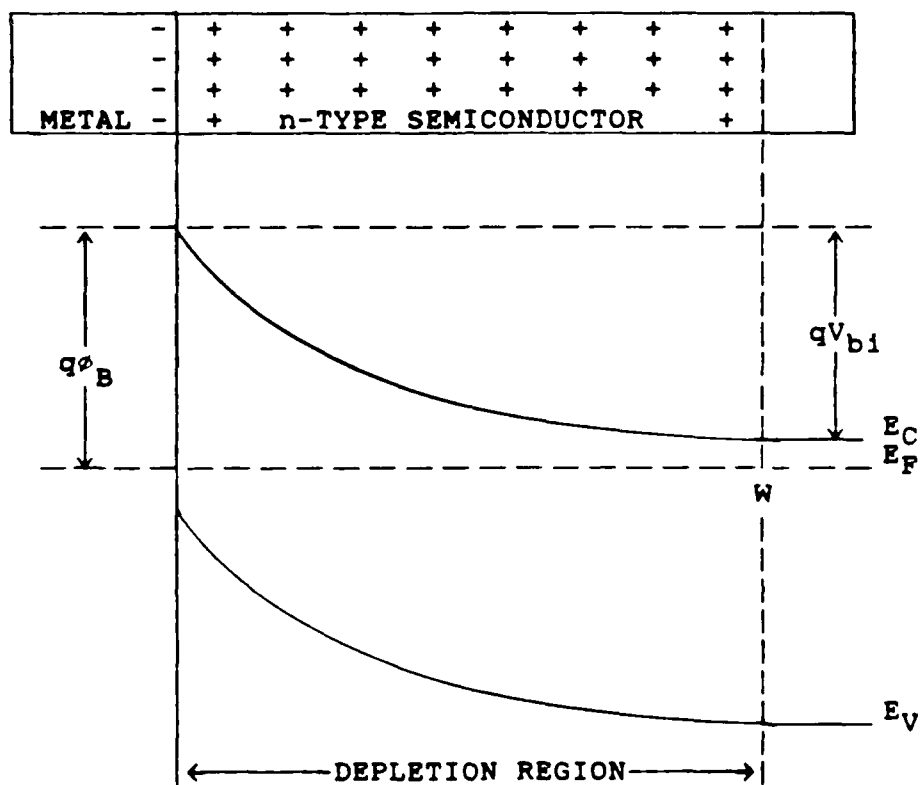
Figure 3.   Energy Band Diagram for a Metal-
            Semiconductor Contact

metal surface to W, so W is called the depletion width.
Chandra et al (7:646) showed that the difference between the
conduction band minimum and the Fermi level is given by

$$E_C - E_F = kT \ln\left[N_C/N(W)\right], \tag{2.2}$$

where k is the Boltzmann constant, T is the temperature, $N_C$
is the density of states at the conduction band minimum, and
N(W) is the carrier concentration at the depletion width W.
The carrier concentration is

$$N = N_D - N_A - n + p, \tag{2.3}$$

where $N_D$ is the donor impurity concentration, $N_A$ is the
acceptor concentration, n is the electron concentration, and
p is the hole concentration. The electron and hole
concentrations are negligible where $N_D - N_A$ is high. The
built-in potential is then

$$V_{bi} = \phi_B - (kT/q)\ln\left[N_C/(N_D-N_A)\right]. \tag{2.4}$$

According to Shottky (8:4), the built-in potential $V_{bi}$
should be the difference between the work functions of the
metal and the semiconductor, $V_{bi} = \phi_M - \phi_{SC}$. However,
experiments showed that the rectification of metal-
semiconductor contacts can be independent of the metal work
function. In 1947, Bardeen (9:5) showed that the surface
barrier potential $\phi_B$ is determined by surface states. The
surface states produce the potential even without a metal
contact. As explained by McKelvey (10:485), the Soviet
physicist Tamm showed in 1932 that the surface states are

9

caused by the ending of a periodic potential, such as the
Kronig-Penney square well potential, by a surface potential
barrier, as shown in Figures 4 and 5.  These additional
states within the forbidden energy band of the Kronig-Penney
model are the discrete allowed energy levels of wave
functions localized near the surface.  Shockley (11)
calculated that there is one surface state for each surface
atom.  Surface states can also be created by impurity atoms,
oxide layers, and surface imperfections.  Treating the
surface electronic states as unfilled orbitals or dangling
bonds, Massies et al (12:64) experimentally observed the
electron transition of a Ga 3d orbital to a dangling Ga bond
on the (100) face of GaAs.  The charging of the surface
states causes the conduction band minimum and the valence
band maximum to rise as they approach the surface, as shown
in Figure 3.  Henisch (13:184) explains that the Fermi level
also rises to the surface, but when the semiconductor is
brought to the metal, its Fermi level falls to equal the
Fermi level of the metal.  This creates an electric field
between the metal and the semiconductor.  If the density of
surface states is large enough to take any additional
charges that would be caused by the electric field, without
much changing the Fermi level, then the space charge in the
semiconductor is unaffected by the metal contact, and the
barrier height potential is independent of the metal work
function (13:184).
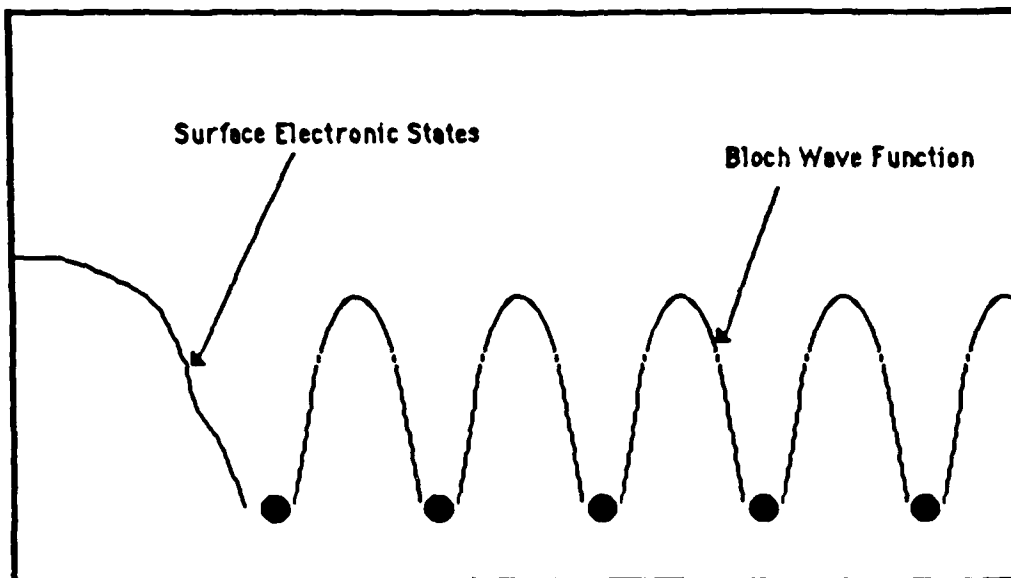
Figure 4. The Kronig-Penney Periodic Potential with Asymmetric Potential at the Crystal Surface
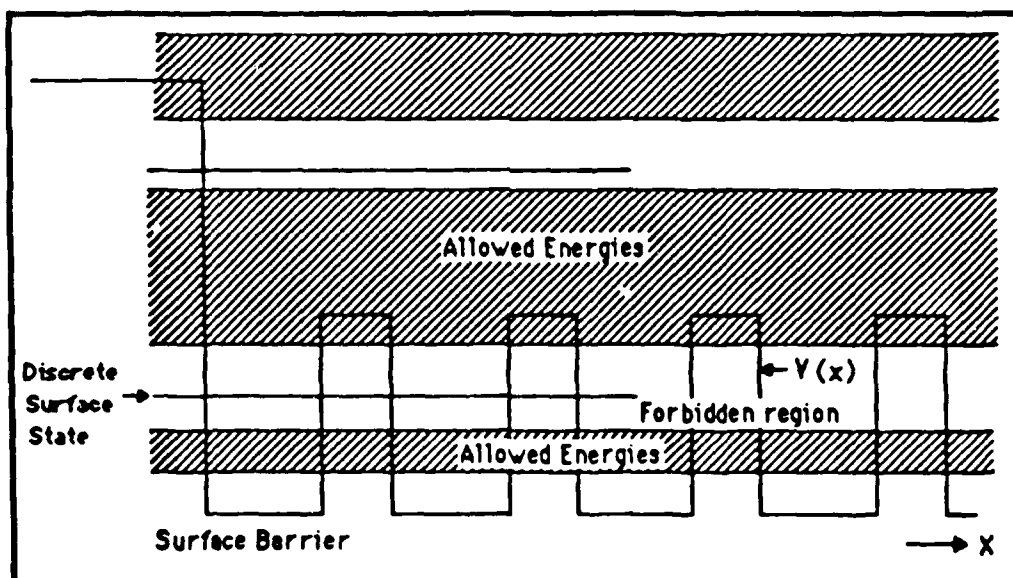


Figure 5. The Formation of Localized States in the Forbidden Energy Region at the Surface of a 1-D Crystal (10:486)

## Capacitance-Voltage Profiling

When a metal and an n-type semiconductor are brought
together, a space charge or depletion region is formed as
shown in Figure 3. When a reverse bias voltage is applied
to the contact, more electrons leave the semiconductor to
the metal, extending the depletion width W deeper into the
semiconductor as shown in Figure 6. In Figure 6, $E_{FM}$ is the
Fermi level in the metal, and $E_{FS}$ is the Fermi level at the
depth W within the semiconductor. The space charge region
can be treated as a voltage dependent parallel plate
capacitor, with capacitance

$$C = \epsilon A/W, \qquad (2.5)$$

where C is the capacitance in Farads, $\epsilon$ is the permittivity
of the material in Farads/cm, A is the area of the metal
contact in $cm^2$, and W is the depletion width in cm. As the
applied bias voltage V increases, W increases, and C
decreases.

In 1942, Schottky had the idea of using capacitance
measurements to obtain dopant profiles (14). Copeland (15),
Miller (16), and Nakhamanson (17) improved upon Schottky's
idea to obtain the following equations for dopant profiles:

$$N(x) = \frac{-C^3}{\epsilon qA^2(dC/dV)} \quad \text{at } x = \epsilon A/C, \qquad (2.6)$$

where $N(x)$ is the carrier concentration at depth x below the
semiconductor surface. The bias voltage is increased in
small increments, and the capacitance is measured for each
voltage to obtain dC/dV at each capacitance.

12

```
        METAL -| +    n-TYPE SEMICONDUCTOR    +    +
```

$$q\phi_B$$

$$q(V_{bj}+V)$$

$$E_{FM}$$

$$E_C$$

$$E_{FS}$$

W

DEPLETION WIDTH

$$W = A\epsilon/C$$

$$N(W) = \frac{-C^3}{\epsilon qA^2 (dC/dV)}$$
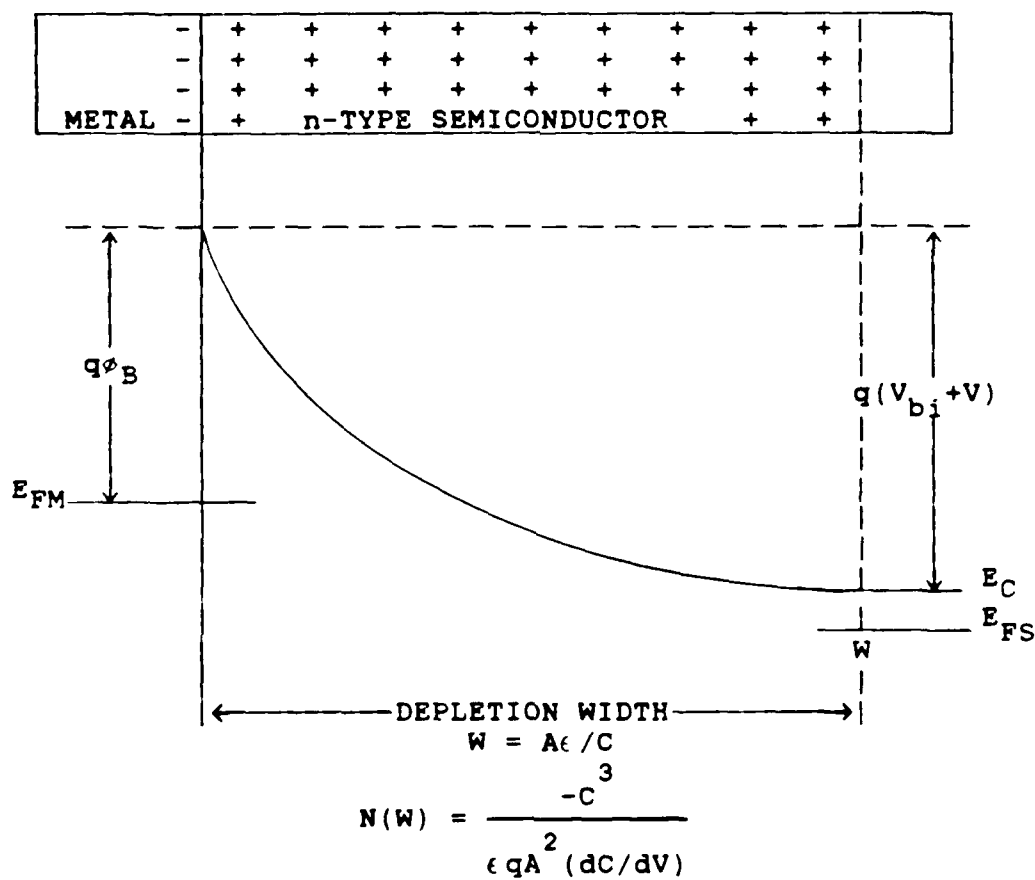
Figure 6.   Depletion Region Due to a Metal-
Semiconductor Contact with Applied Bias

13

To measure the capacitance, the bias voltages are actually superimposed upon an alternating voltage at frequency $\omega$. The measured capacitance is

$$C' = C/(1-\omega^2 r^2 C^2), \qquad (2.7)$$

where C is the actual depletion layer capacitance, and r is a series resistance within the semiconductor (16:1106). $\omega r C$ is made small so that C' is approximately C. This is done by reducing the metal contact area to reduce C, requiring r to be small in the semiconductor, and making $\omega$ as small as possible without ruining the signal-to-noise ratio. The frequency must also be high compared to the relaxation times of traps in the semiconductor (16:1106). Traps hold on to electrons much longer than most dopant atoms and distort the measured profile. The best frequency for GaAs is usually about 1MHz.

This C-V profiling method has the advantages that 1) it measures only the electrically active impurity concentration, 2) it is completely automated, and 3) it is non-destructive. The C-V method has the disadvantages that 1) it cannot be used for concentrations above about $10^{18}$ $cm^{-3}$, because voltage breakdowns and current leaks occur, 2) it is practically restricted to n-type semiconductors, and 3) it cannot measure the concentrations within the initial depletion region, which occurs at zero applied bias voltage. The initial depletion region often ends $0.2\mu m$ or deeper into the semiconductor. Applying a forward bias voltage would enable concentration measurements closer to the

semiconductor surface, except that at even small forward

bias voltages a diffusion capacitance becomes too great

(18:94). This paper explains a method of combining C-V

measurements with the etching of layers from the

semiconductor surface to measure the charge carrier

concentrations within the initial depletion region.

# III. Experiments

## Sample Preparation

The samples used in this study were prepared and doped before the study began. The substrate materials used in the study were <100> oriented undoped or Cr-doped semi-insulating GaAs. The samples were originally cut into 1/4 inch squares from 2 inch curcular wafers of the GaAs. Prior to implantation, each sample was cleaned with basic-H, de-ionized water, trichloroethylene, acetone, and methanol, and dried with blowing nitrogen gas. Then, the substrate was free-etched with an $H_2SO_4:30\%H_2O_2:H_2O$ solution in a 7:1:1 ratio by volume for 3 minutes. The samples were then ion implanted with Si at room temperature with an incident energy of 100 or 200 keV for a dose of $8x10^{12}$ or $1x10^{13}$ ions/$cm^{-2}$. The ion beam was directed at 7 degrees off the <100> crystal axis to minimize ion channeling. After implantation, the samples were soaked in an HCl solution for 1 minute to remove a natural oxide layer which had grown since implantation. The samples were then immediately

capped with a 1000 Å layer of $Si_3N_4$ using a pyrolytic deposition system. Next, the samples were annealed at 800 or 850 °C for 15 minutes in flowing hydrogen gas to activate the implanted ions. This produces high activation efficiencies, as shown by Kim (19:27), who achieved activation efficiencies of at least 80% for $6x10^{12}$ $cm^{-2}$

16

Si-implants in GaAs. After annealing, the encapsulants were removed with a 48% hydrofluoric acid solution, which required about 5 minutes. Each half inch square sample was then cut into 4 quarter inch square samples.

## C-V Measurements and Etching

A series of concentration profiles was measured for each Si implanted GaAs sample using the C-V technique. The samples were etched between the capacitance and voltage measurements to find the carrier concentrations within the initial depletion region of each sample. About ten etches were performed on each sample to acquire C-V data throughout the initial depletion region. The samples were cleaned before each set of capacitance and voltage measurements, because it was found that the cleaning could very much affect the measurements, especially if a sample was not cleaned for several days.

The C-V data was obtained using the Hewlett-Packard Model 4061 Semiconductor/Component Test System, which was controlled by a 9845B H-P Computer. A sample to be profiled was placed with the implanted face down onto a suction chuck as shown in Figure 7. The suction chuck has three ducts. One duct pulls the air out of a circular groove on the chuck creating a vacuum between the chuck and the sample. Actually, the samples were too small to cover the circular groove, so a sheet of plastic had to be placed over the test chuck and pressed down around the circular groove to obtain

17

Semiconductor
Sample

Chuck

Vacuum Passage
Hole
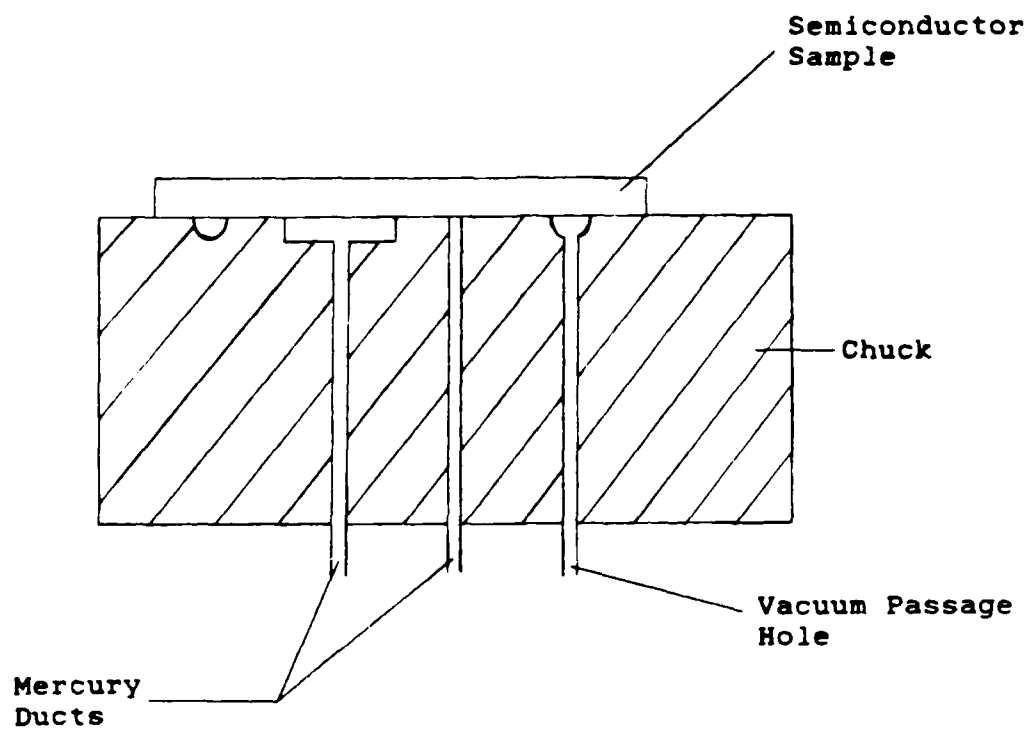
Mercury
Ducts

Figure 7. Cross Section of Mercury Contacts

a vacuum between the test chuck and the sample. This vacuum pulls the sample down to the chuck and pulls mercury up the other two ducts. The two mercury columns then make metal contacts with the test sample. One mercury duct has a much larger contact area, and it was connected to the high side of the bias supply. The smaller mercury duct was connected to the low side. Bias voltages from 0 to -5 or -10 volts were incrementally applied to the sample. The bias voltages were supplied by the Hewlett-Packard 4140B DC Voltage Source. The 4275A Multi-Frequency LCR Meter supplied a 0.01 V, 1 MHz test signal to measure the complex impedance and determine the capacitance of an assumed equivalent circuit. The circuit had the capacitance of the space charge region, or depletion region, in series with the resistance of the material between the two mercury contacts. The capacitance of the larger mercury contact area is much greater than that of the smaller mercury duct contact area, so the measured capacitance is approximately equal to the actual depletion region capacitance. C-V measurements were taken at two positions on each sample, and it was found that the measurements could change somewhat with the location of the mercury contact area. The C-V measurements were stored on tape in data files, which were transferred to the AFIT computer system.

Between the C-V measurements, etching was performed with an $H_2SO_4:30\%H_2O_2:H_2O$ solution in a 1:1:500 ratio by volume, at room temperature and with constant stirring.

This solution etched about 80 Å per minute. Alongside the
sample to be etched, two control samples were also etched.
The control samples were half coated with black wax, and the
black wax was not removed until after the last etching.
Since the control samples were not etched under the black
wax, a step height could be measured on these samples as a
total etched depth, and thus, the etch rate could be
determined. The etched depth was measured using the
Sloan-Dektak IIA Surface Profiling System.

# IV. Theory

Three methods were developed for determining the charge carrier concentration within the initial depletion region. They are the Charge Density Moment Method, the Voltage Second Derivative Method, and the Voltage First Derivative Method. The Voltage Second Derivative Method is the best mathematically, but the Voltage First Derivative Method is much less sensitive to experimental error.

## Charge Density Moment Method

When a metal is brought into contact with an n-type semiconductor under a reverse bias applied voltage V, the potential $\psi$ varies with depth into the semiconductor as shown in Figure 8. The potential falls off steeply and then levels off at a distance $x_W$. $\phi_B$ is the barrier potential. $E_C$ is the conduction band minimum at $x_W$, and $E_{FS}$ is the Fermi energy level at $x_W$. q is the electronic charge. $V_{bi}$ is the built-in potential. The depletion region extends from $x = 0$ to $x = x_W$. As seen by equation (2.4), the built-in potential depends on the endpoints $x = 0$ and $x = x_W$. The potential $\psi$ is governed by Poisson's equation:

$$-\frac{d^2\psi}{dx^2} = \frac{\rho(x)}{\epsilon} = \frac{qN(x)}{\epsilon} = \frac{dE}{dx} , \qquad (4.1)$$

where $\rho(x)$ is the charge density at x, $\epsilon$ is the permittivity of the semiconductor, $N(x)$ is the carrier concentration given by equation (2.3) at x, and E is the electric field.
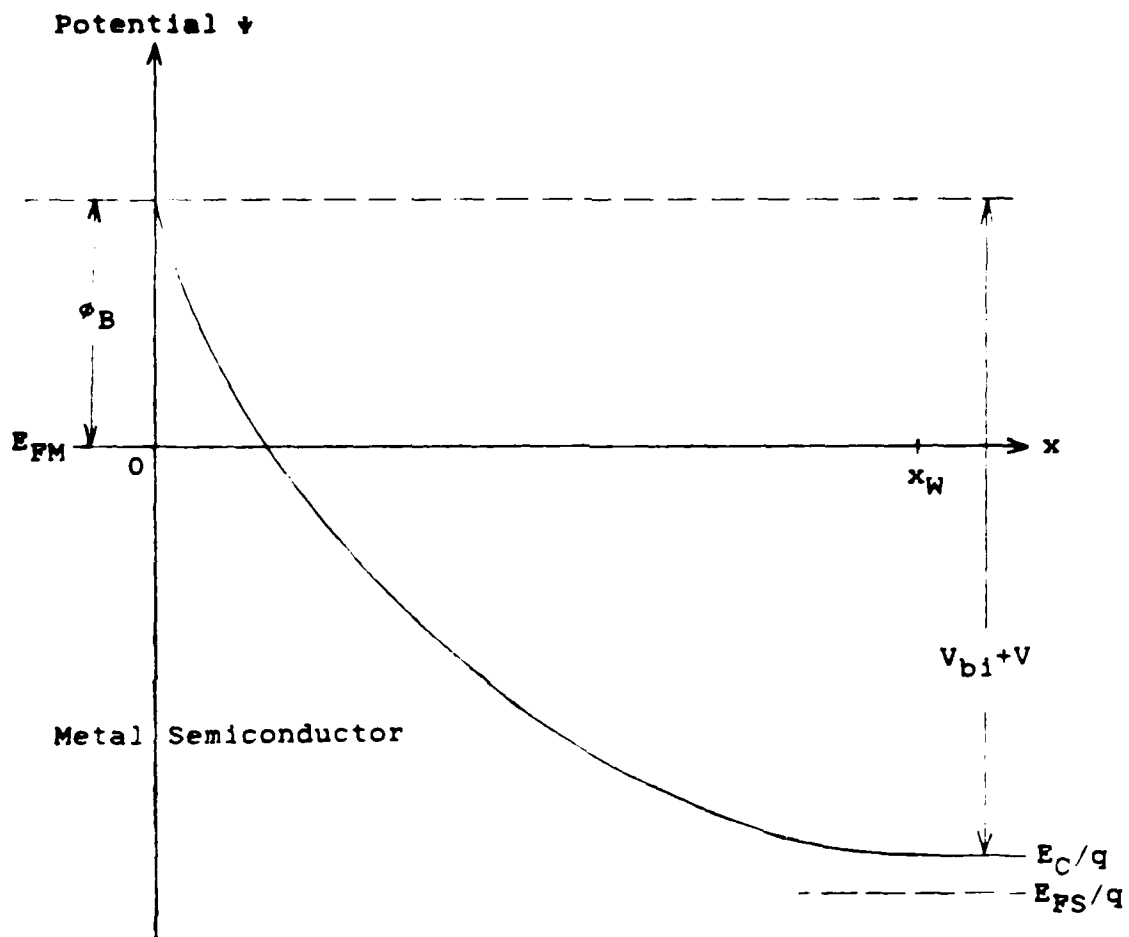
21

Figure 8. Potential Diagram of Metal-Semiconductor Contact

By integrating Poisson's equation once, the electric field is found to be

$$E(x) = \frac{q}{\epsilon} \int_x^{x_W} N(x)dx + E_W, \qquad (4.2)$$

where $E_W$ is the electric field at $x_W$ (20:209). This is the same result that would be obtained using Gauss' Law, since the integral term contains the total charge per area from x to $x_W$. By integrating a second time, the voltage drop from the surface to $x_W$ is shown to be

$$V + V_{bi} = \frac{q}{\epsilon} \int_0^{x_W}\int_x^{x_W} N(x)dxdx + x_W E_W, \qquad (4.3)$$

where V is the applied reverse bias voltage required to extend the depletion region to $x_W$, and the reverse bias voltages are considered positive. Giacoletto (20:210) pointed out that this *double integral* can be integrated by parts to yield

$$V + V_{bi} = \frac{q}{\epsilon} \int_0^{x_W} xN(x)dx + x_W E_W, \qquad (4.4)$$

which relates the applied voltage to a moment of the charge density. If the depletion region is assumed to end abruptly as shown in Figure 9, then $E_W$ is zero, since there are no charges right of $x_W$. Actually, the depletion region ends gradually, as shown in Figure 10, due to an electron "tail" at $x_W$ (18:74-77). The electron concentrations near $x_W$ are usually considered small and the abrupt approximation applied, so that $E_W$ is considered negligible (21:790). With the $E_W$ term dropped off, the above equation is
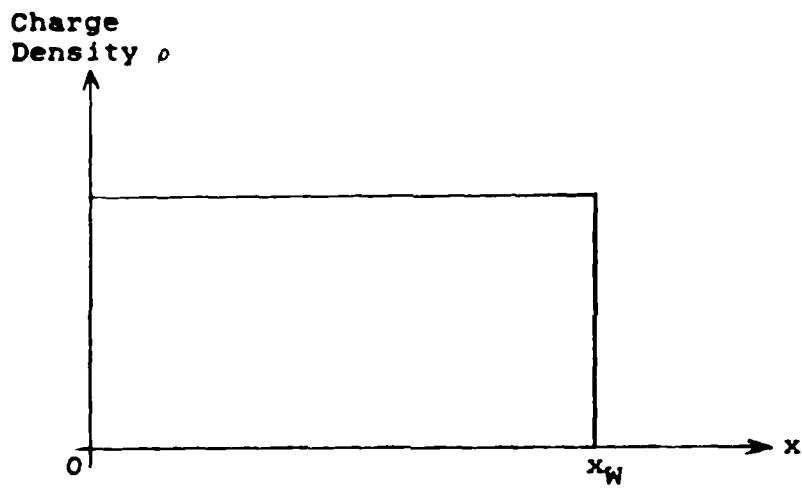
23

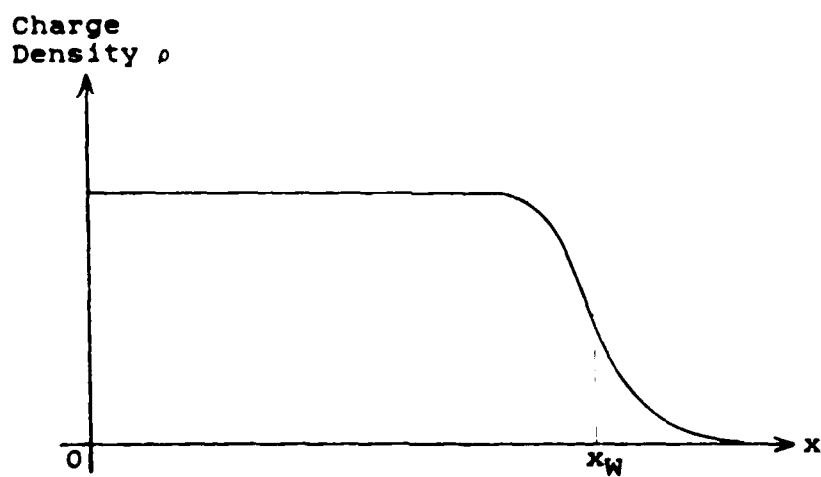Figure 9. Abrupt Approximation of Depletion Region



Figure 10. Gradual Ending of Depletion Region

$$V + V_{bi} = \frac{q}{\epsilon} \int_0^{x_W} x N(x) \, dx. \qquad (4.5)$$

From this equation, it can be seen that even if one measures V, $V_{bi}$, and $x_W$, an infinite number of N(x) profiles could give the same result. There is no unique N(x) profile that satisfies equation (4.5).

Giacoletto (20:215) also showed that the voltage drop from a position $x_0$ to $x_W$ is

$$\psi(x_0) - \psi(x_W) = \frac{q}{\epsilon} \int_{x_0}^{x_W} (x - x_0) N(x) \, dx + (x_W - x_0) E_W, \qquad (4.6)$$

where $x_0$ is between 0 and $x_W$. If $x_W$ is far from both x=0 and $x=x_0$, then $E_W$ and the shape of the space charge region (as shown in Figure 10) should change very little with etching of the semiconductor between the surface and $x_0$. Under these circumstances, it can be seen from equation (4.6), that the potential drop from $x_0$ to $x_W$ is the same regardless of whether material has been etched away between 0 and $x_0$. In that case,

$$V(x_0, x_W) + V_{bi}(x_0, x_W) = \psi(x_0) - \psi(x_W), \qquad (4.7)$$

where $V(x_0, x_W)$ and $V_{bi}(x_0, x_W)$ are respectively the applied voltage and built-in potential when the depletion region extends from an etch depth of $x_0$ to $x_W$.

If one designates the ith etch thickness as $t_i$ and the distance of the ith etched surface from the original unetched surface as $T_i$, then

25

$$T_i = \sum_{j=0}^{i} t_j \text{ and } T_0 = 0. \tag{4.8}$$

The potential difference between $T_i$ and $x_W$ is

$$V(T_i, x_W) + V_{bi}(T_i, x_W) = \frac{q}{\epsilon} \int_{T_i}^{x_W} (x - T_i) N(x) dx + (x_W - T_i) E_W(T_i, x_W).$$

$$\tag{4.9}$$

where $E_W(T_i, x_W)$ is the electric field at $x_W$ when the depletion region starts at the etch depth $T_i$, and $x_W$ is given by

$$x_W = \epsilon A / C(T_i, x_W). \tag{4.10}$$

$C(T_i, x_W)$ is the capacitance measured when the applied bias voltage is $V(T_i, x_W)$. There are various ways equation (4.9) can be used to find the concentration $N(x)$ within the initial depletion region. The voltage drop from the etch depth $T_{i-1}$ to $x_W$ is

$$V(T_{i-1}, x_W) + V_{bi}(T_{i-1}, x_W) = \frac{q}{\epsilon} \int_{T_{i-1}}^{x_W} (x - T_{i-1}) N(x) dx +$$

$$+ (x_W - T_{i-1}) E_W(T_{i-1}, x_W). \tag{4.11}$$

As shown by equation (2.4), the built-in potential $V_{bi}$ depends on the etch surface barrier potential $\phi_B$ and the carrier concentration $N(x_W)$ at $x_W$. If one assumes that the surface barrier potential $\phi_B$ is the same for each etch depth, and if $x_W$ is used as a common reference, then the built-in potentials are the same:

$$V_{bi}(T_i, x_W) = V_{bi}(T_{i-1}, x_W). \tag{4.12}$$

26

As described earlier, the electric field at $x_W$ changes
little with a change in the etch depth, especially if $x_W$ is
far from the etch surfaces. The electric field at $x_W$ is
usually considered as near zero anyway. Therefore,
subtracting equation (4.9) from equation (4.11) yields

$$V(T_{i-1},x_W)-V(T_i,x_W) = \frac{q}{\epsilon}\int_{T_{i-1}}^{x_W}(x-T_{i-1})N(x)dx - \frac{q}{\epsilon}\int_{T_i}^{x_W}(x-T_i)N(x)dx,$$

$$(4.13)$$

which can be expressed as

$$\int_{T_{i-1}}^{T_i}(x-T_{i-1})N(x)dx =$$

$$\frac{\epsilon}{q}\left[V(T_{i-1},x_W) - V(T_i,x_W)\right] - (T_i-T_{i-1})\int_{T_i}^{x_W}N(x)dx. \qquad (4.14)$$

With the Nth etch depth $T_N$ as the distance to the end of the
initial depletion region of the original unetched surface,
as shown in Figure 11, then

$$\int_{T_{N-1}}^{T_N}(x-T_{N-1})N(x)dx =$$

$$\frac{\epsilon}{q}\left[V(T_{N-1},x_W) - V(T_N,x_W)\right] - (T_N-T_{N-1})\int_{T_N}^{x_W}N(x)dx. \qquad (4.15)$$

The quantities on the right side of equation (4.15) are all
measurable or known. If the etch thicknesses are small, the
concentration $N(x)$ can be treated as uniform or constant
between $T_{N-1}$ and $T_N$. Using $t_N$ for the Nth etch thickness

27
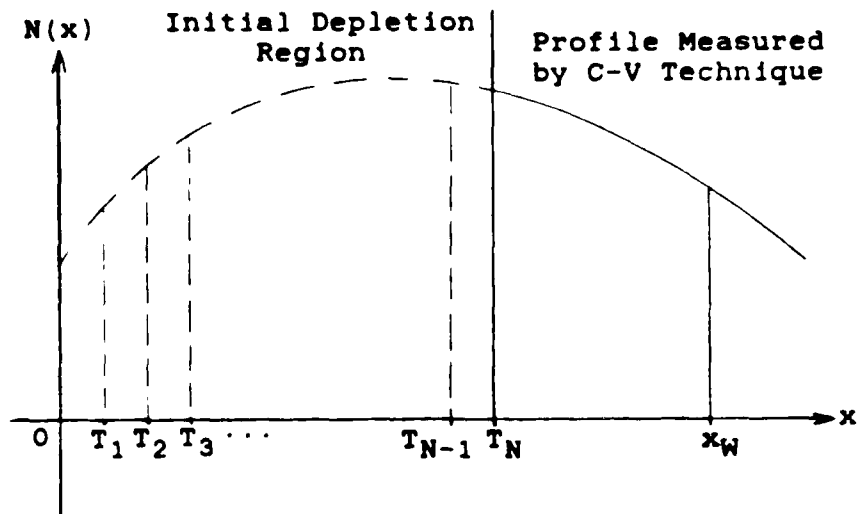
Figure 11. Etch Depths Across Carrier Profile

between the etch depths, the integral on the left side can
then be evaluated and the equation solved for N to give

$$N \cong \frac{2}{t_N^2} \left\{ \frac{\epsilon}{q} \Big[ V(T_{N-1}, x_W) - V(T_N, x_W) \Big] - t_N \int_{T_N}^{x_W} N(x) dx \right\} , \qquad (4.16)$$

and this value of N can be assigned to the midpoint of the
two etch depths:

$$x = \frac{T_{N-1} + T_N}{2} . \qquad (4.17)$$

With $N(x)$ known between $T_{N-1}$ and $T_N$, the same method can
then be applied to find $N(x)$ between $T_{N-2}$ and $T_{N-1}$. This
method can be repeatedly applied working backward to the
original unetched surface.

28

Since this method treats the concentration as uniform between each pair of etch depths, its values of the concentrations will be slightly different from the true values. If the value calculated for the concentration within one etch layer is smaller than the true value, the calculated value in the next etch layer will compensate by being higher than its true value. Thus, the concentrations calculated by this method oscillate about the true profile. In this case, a best fit curve should be obtained. Another disadvantage of this method is that it cannot be applied until after etching to the end of the initial depletion region.

## Voltage Second Derivative Method

As explained in the previous section, the basic shape of the space charge region should stay nearly constant from one etch depth to the next, if $x_W$ is far from the etch depths and the etch thickness is small. Then, equation (4.7) can be used, and

$$V(T_i, x_W) = \psi(T_i) - \psi(x_W) - V_{bi}(T_i, x_W). \qquad (4.18)$$

Furthermore, if $x_W$ is used as a common reference distance for each etch depth, $\psi(x_W)$ and $V_{bi}(T_i, x_W)$ can be treated as constants. Then, the applied voltage is the potential difference above $\psi(x_W) + V_{bi}$, as shown in Figure 12. Consequently, equation (4.1) can be used to find the

29

concentration:

$$N(x) = \frac{-\epsilon}{q} \frac{d^2 V}{dx^2} \ .$$ 

(4.19)
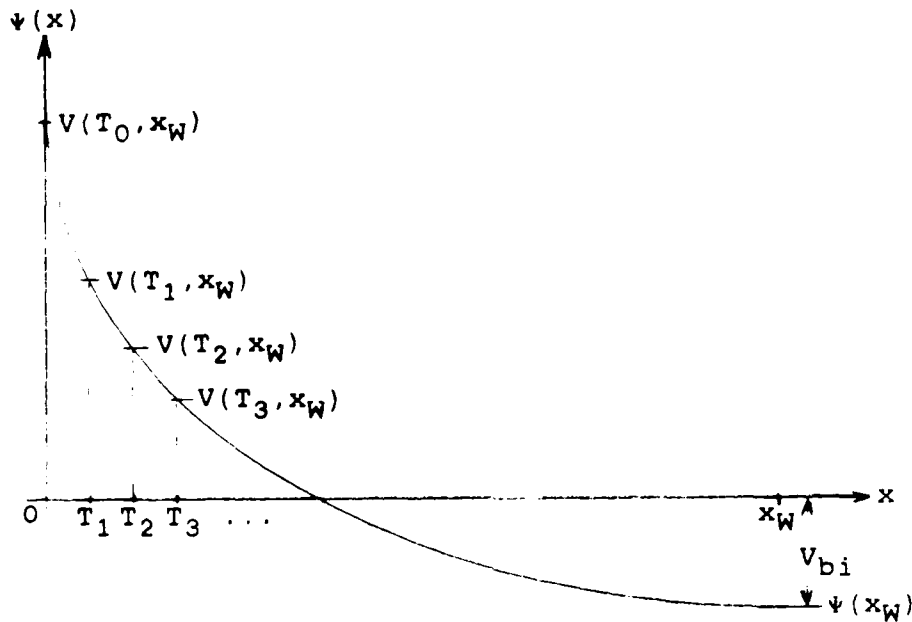


Figure 12. Potential Versus Etch Depth

Considering the reverse bias voltages as positive, and expressing the voltage second derivative in terms of etch thicknesses and etch depths, the concentration is

$$N \cong \frac{2\epsilon}{q(t_i + t_{i+1})} \left[ \frac{V(T_{i-1}, x_W) - V(T_i, x_W)}{t_i} - \frac{V(T_i, x_W) - V(T_{i+1}, x_W)}{t_{i+1}} \right] ,$$

(4.20)

and this value of N can be assigned to the midpoint of the two etch layers:

$$x = \frac{T_{i-1} + T_{i+1}}{2} \ .$$

(4.21)

It can be mathematically shown that equation (4.20) gives a
value of the concentration which is between the minimum and
maximum values of $N(x)$ in the range between $T_{i-1}$ and $T_{i+1}$,
if the measured voltages and thicknesses are exact.
However, since equation (4.20) is based on a second
derivative, it is very sensitive to experimental error.
Much higher accuracy can be obtained by smoothing the curve
of the voltage first derivative and then taking the
derivative of this curve to obtain the voltage second
derivative. Further accuracy can be obtained by using small
etch thicknesses and averaging $N(x)$ over a range of $x_W$'s.
This Voltage Second Derivative Method is much simpler than
the Charge Density Moment Method and can be immediately
applied after the first two etches (three, counting the
zeroth etch).

## Voltage First Derivative Method

By Gauss' Law, the electric field at a depth within the
semiconductor is proportional to the charge per area past
that depth:

$$E(x) = \frac{q}{\epsilon} \int_x^\infty N(x)\,dx. \qquad (4.22)$$

If one assumes that most of the charge is within the the
depletion width, then

$$E(x) = \frac{q}{\epsilon} \int_x^{x_W} N(x)\,dx, \qquad (4.23)$$

31

where $x_W$ is the end of the depletion region. The average value of $N(x)$ between $x$ and $x_W$ is

$$N_{av}(x, x_W) = \frac{\int_x^{x_W} N(x)\,dx}{(x_W - x)} = \frac{\epsilon}{q}\, \frac{E(x)}{(x_W - x)} \quad . \tag{4.24}$$

As illustrated in Figure 12, the derivative of the potential is the derivative of the applied voltage which extends the depletion region from an etch depth $x$ to $x_W$. The electric field at $x$ is then

$$E(x) = -\frac{d\psi}{dx} = -\frac{dV}{dx} \quad . \tag{4.25}$$

In terms of etch depths and thicknesses, the electric field is

$$E\left(x = \frac{T_i + T_{i+1}}{2}\right) \cong -\frac{\left[V(T_{i+1}, x_W) - V(T_i, x_W)\right]}{t_{i+1}} \quad . \tag{4.26}$$

Substituting the electric field of equation (4.26) into equation (4.24) gives

$$N_{av}\left(\frac{T_i + T_{i+1}}{2}, x_W\right) \cong \frac{\epsilon}{q}\, \frac{\left[V(T_i, x_W) - V(T_{i+1}, x_W)\right]}{t_{i+1}\left(x_W - \frac{T_i + T_{i+1}}{2}\right)} \quad . \tag{4.27}$$

This average value of $N$ can be assigned to the midpoint of the range of its average:

$$x = \left[\frac{T_i + T_{i+1}}{2} + x_W\right]/2 = (T_i + \frac{t_{i+1}}{2} + x_W)/2 \quad . \tag{4.28}$$

This is the Voltage First Derivative Method. It is a crude

approximation, and it approximates the concentrations only in the second half of the depletion region, but it is much less sensitive to experimental error than the Voltage Second Derivative Method. Also, the value of N throughout the initial depletion region can be calculated more precisely by using the Voltage First Derivative Method as a first step of the Voltage Second Derivative Method, as described below.

The value of N between etch layers can be determined by using sheet-carrier concentrations. The sheet-carrier concentration $N_s(x_0, x_W)$ is the total charge carriers per area from $x_0$ to $x_W$. The sheet-carrier concentration is given by

$$N_s(x_0, x_W) = N_{av}(x_0, x_W)(x_W - x_0) . \qquad (4.29)$$

The concentration between depths $x_0$ and $x_1$ can be determined from

$$N\left(x = \frac{x_0 + x_1}{2}\right) \cong N_{av}(x_0, x_1) = \frac{N_s(x_0, x_W) - N_s(x_1, x_W)}{(x_1 - x_0)} . \qquad (4.30)$$

By using equations (4.29) and (4.30), the value of N between etch layers can be obtained from

$$N\left(x = \frac{T_{i-1} + T_{i+1}}{2}\right) \cong$$

$$\frac{N_{av}\left[\frac{T_{i-1} + T_i}{2}, x_W\right]\left(x_W - \frac{T_{i-1} + T_i}{2}\right) - N_{av}\left[\frac{T_i + T_{i+1}}{2}, x_W\right]\left(x_W - \frac{T_i + T_{i+1}}{2}\right)}{(T_{i+1} - T_{i-1})/2}.$$

$$(4.31)$$

By using equation (4.27) for the average concentrations in equation (4.31), equation (4.20) is obtained, so the Voltage Second Derivative Method is based on the Voltage First Derivative Method. Therefore, inaccuracies and experimental error in the Voltage First Derivative Method appear much larger in the Voltage Second Derivative Method. If the average concentrations calculated using equation (4.27) are curve fit or smoothed, then good results can be obtained using equation (4.31).

## V. Computer Programs

Computer programs were written to implement the methods developed in the previous section and use capacitance-voltage data to calculate the carrier concentrations within the initial depletion region. To better analyze these methods, files of ideal capacitance-voltage data were computer generated for various dopant distributions. C-V equations (2.6) could be applied in reverse to create the ideal data, but it was found that the C-V equations can be derived from the differential form of equation (4.5):

$$dV = \frac{q}{\epsilon} xN(x)dx \qquad (5.1)$$

by using

$$C = \epsilon A/x \ . \qquad (5.2)$$

These equations (5.1) and (5.2) were used to generate the ideal C-V data. Since equations (5.1) and (5.2) are the same type of equations used in developing the methods of finding the initial depletion region concentrations, the methods could not be proven using the ideal computer generated C-V data. However, it is assuring that the methods are based on the same assumptions as the regular C-V technique, and the ideal data could still be used in analyzing the methods and the effects of experimental error. The capacitances after the ith etch were easily calculated as

35

$$C(i,j) = \epsilon A/(x_j - T_i), \qquad (5.3)$$

where $C(i,j)$ is the jth capacitance after the ith etch and $x_j$ is the jth distance from the original unetched surface.

$$x_j = T_i + jh, \qquad (5.4)$$

where h is a small distance interval. Similar to equation (5.1), the voltages were determined from

$$V(i,j) - V(i,j-1) = \frac{-q}{\epsilon} \, jh \, \frac{\left[N(x_j) + N(x_j - h)\right]}{2} \, h \,, \qquad (5.5)$$

where $V(i,j)$ is the jth total voltage after the ith etch, considering reverse bias voltages as negative. A constant built-in potential of 0.8 V was assumed throughout the calculations for the ideal C-V data, so the zeroth voltage was set at 0.8: $V(i,0) = 0.8$ . The voltage increments were added to this starting voltage to obtain the applied bias voltages. The voltage and capacitance pairs with voltages less than or equal to 0, were stored in a data file for the ith etch. Usually, 11 data files were made for 10 etches, 100 Å each.

To calculate the concentrations from the data files by the regular C-V technique, the finite difference form of equation (2.6) was used:

$$N(x) = \frac{\left[V(i,j-1) - V(i,j)\right]}{\epsilon q A^2 \left[C(i,j) - C(i,j-1)\right]} \left[\frac{C(i,j) + C(i,j-1)}{2}\right]^3, \qquad (5.6)$$

where

$$x = T_i + \frac{2\epsilon A}{\left[C(i,j) + C(i,j-1)\right]} \ . \tag{5.7}$$

As expected, the profiles calculated by this C-V technique, for the different etches, overlapped exactly for the ideal C-V data. For the experimental data, the profiles for the different etches overalapped only approximately, as shown in Figures 26 to 37.

The computer programs used to find the depletion region concentrations all required a measure of $V(T_i, x_W)$, the applied voltage necessary to extend the depletion region from the etch depth $T_i$ to the common reference distance $x_W$. The distances from the original unetched surface to the edge of the depletion region were given by

$$D(i,j) = T_i + \frac{\epsilon A}{C(i,j)} \ . \tag{5.8}$$

Thus, for each $V(i,j)$, there was an associated distance $D(i,j)$. $V(T_i, x_W)$ could then be found through linear or spline interpolation between these distances.

For the Voltage Second Derivative Method, the concentration at each depth was averaged over a range of common reference distances $x_W$. These ranges were chosen where the C-V profiles overlapped best for the different etches. However, the Voltage First Derivative Method is most accurate when the common reference distance is chosen as close as possible to the original unetched surface, since this narrows the distances over which the concentrations are

37

averaged.  For this reason, each point calculated by the
Voltage First Derivative Method was calculated using only
one common reference distance, which was as close as
possible to the original unetched surface.

# VI. Results and Discussion

## Results for Ideal C-V Data

Figure 14 shows the performance of the Charge Density Moment Method for the ideal C-V data of the LSS Gaussian distribution shown in Figure 13. The calculated concentrations in the initial depletion region oscillated more than expected about the true curve. The amount of oscillation varied with the choice of the common reference distance $x_W$. This was probably because of inaccuracies in the voltage interpolations caused by too large of a step size in generating the ideal data. The Charge Density Moment Method cannot be applied until after etching to the end of the initial depletion region. Also, this method required an integration to find the area under the profile from the edge of the depletion region to the common reference distance. Slight differences in this area could very much affect the results of this method, and the profiles obtained using the regular C-V technique did not overlap well. For these reasons and because of the oscillations about the true profile, this method was not attempted on experimental data.

The Voltage Second Derivative Method worked very well on the ideal data, as shown for the LSS profile of Figure 15, the linear profile of Figure 16, and the parabolic profile of Figure 17. The original LSS profile is shown in

Figure 12, and the original parabolic profile of Figure 17 is shown in Figure 18. In these figures, the first data point calculated by the regular C-V technique after each etch is labeled with the number of the etch. Figure 19 shows the results of the Voltage Second Derivative Method when the voltages of every other etch are purposely offset by 1 mV. This was done to show how sensitive the method is to experimental inaccuracies.

The Voltage First Derivative Method worked much better than expected, as shown for the LSS, linear, and parabolic distributions in Figures 20, 21, and 22, respectively. The concentrations calculated by this method start at the midpoint of the initial depletion region and extend outside the depletion region, almost overlapping the profiles calculated by the regular C-V technique.

Results for Experimental C-V Data

As explained at the end of Section IV, the Voltage Second Derivative Method is based on the Voltage First Derivative Method, so inaccuracies in the latter show up much greater in the former. The results of these two methods should be viewed together. For comparison with these methods, an LSS distribution is shown in Figure 23. The LSS curve is for Si implanted into GaAs at an energy of 100 keV and a dose of $1 \times 10^{13}$ cm$^{-2}$, which was usually used in this study. The results of the two methods are shown in Figures 24 - 33. The Voltage First Derivative Method gave

concentrations starting at the midpoint of the initial

depletion region and then approximately overlapping the C-V

profiles just as demonstrated in Figure 20 for ideal data.

However, the curves calculated by this method were much more

jagged for the experimental data. This jaggedness can be

seen as fluctuations about a true profile, so a smooth curve

can be drawn through these fluctuations. By using the data

of a smooth curve with equation (4.31), which is another

form of the Voltage Second Derivative Method, good results

can be obtained for the concentrations throughout the

initial depletion region. In this way the Voltage First

Derivative Method can be used as a first step of the Voltage

Second Derivative Method. When the Voltage Second

Derivative Method is applied alone, the results can be

erratic, as shown in Figures 25, 26, 28, 30, 31, and 33. A

different common reference distance was used for each point

calculated by the Voltage First Derivative Method, but the

same common reference distance must be used for each point,

when the first derivative method is used as a first step in

the second derivative method. This was tried, but the

calculated data points were too few and the fluctuations too

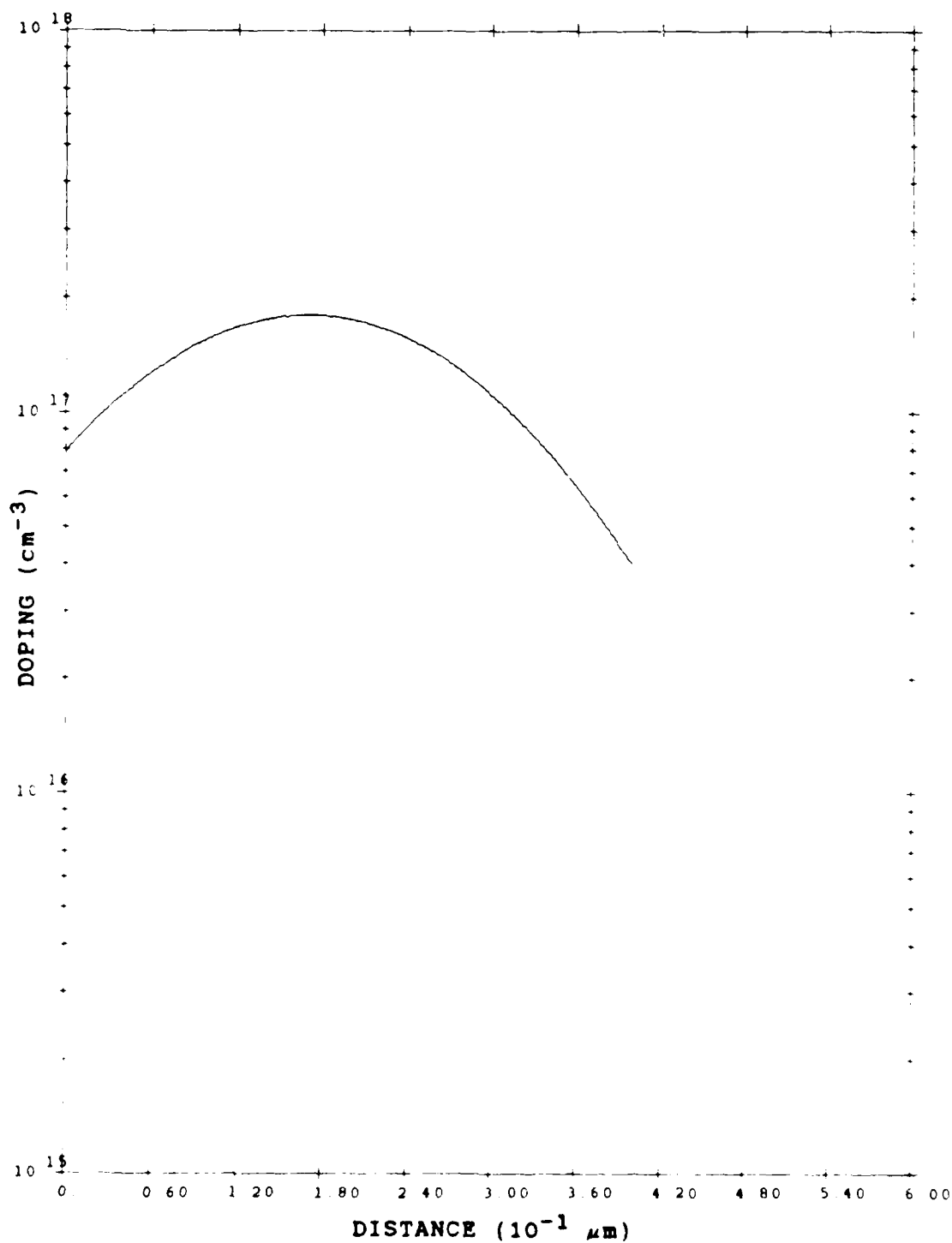large to confidently draw a smooth curve through the

fluctuations.

Figure 13.   An LSS Gaussian Carrier Distribution with a
             Range of 0.17μm and a Standard Deviation
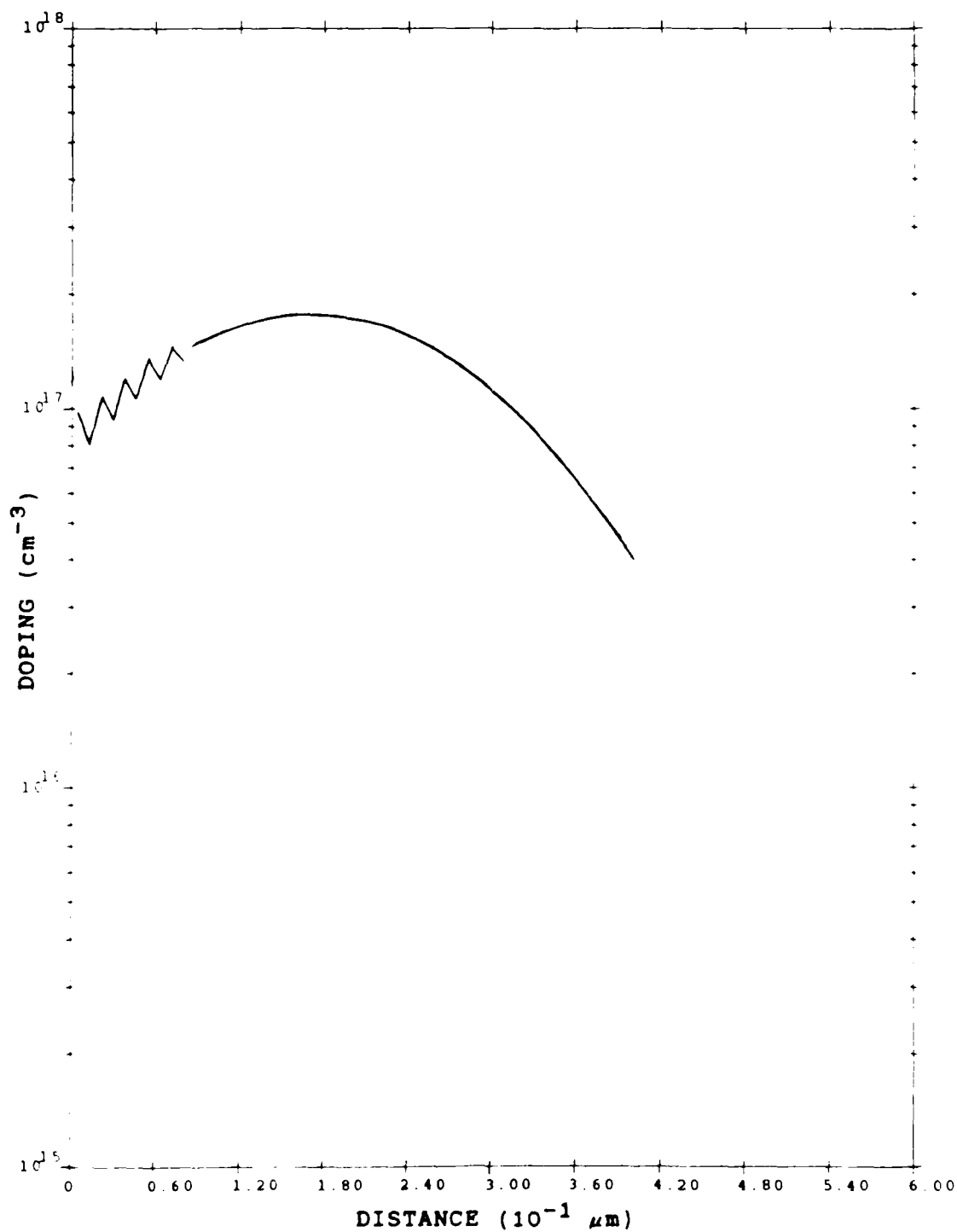             of 0.13μm

42

Figure 14.   Performance of the Charge Density Moment Method
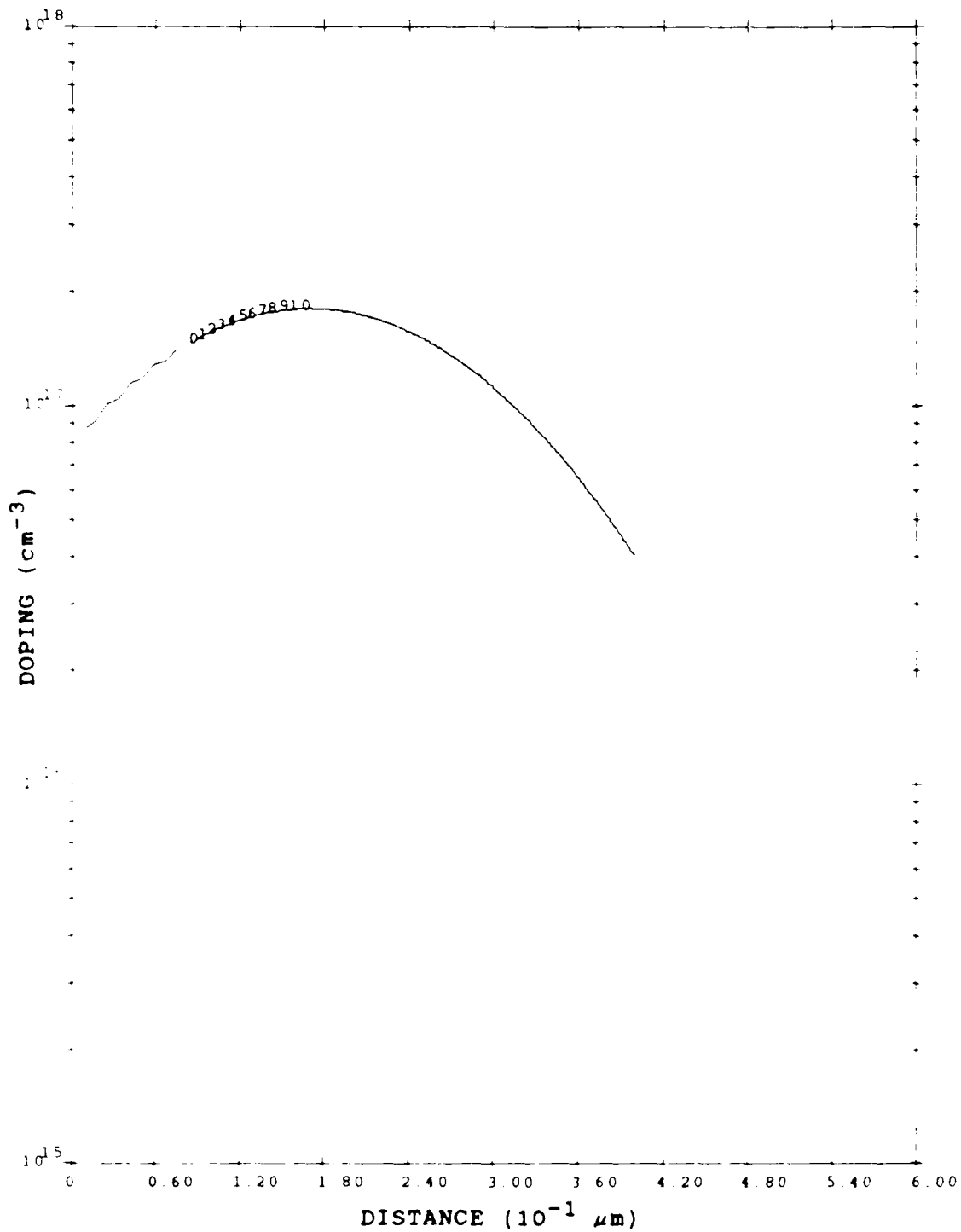for the LSS Profile of Figure 13

Figure 15. Performance of the Voltage Second Derivative
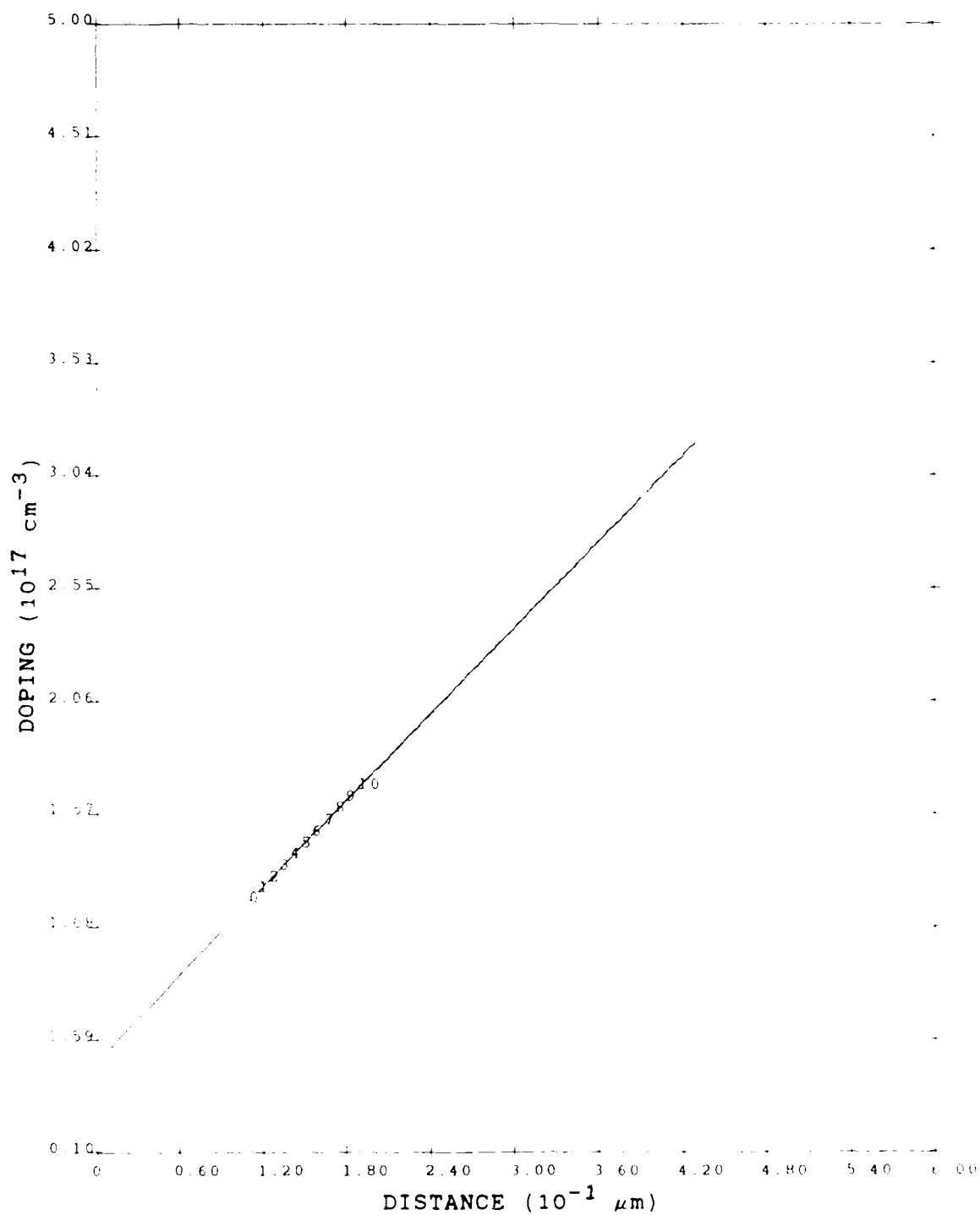Method for the LSS Profile of Figure 13

44

Figure 16. Performance of The Voltage Second Derivative
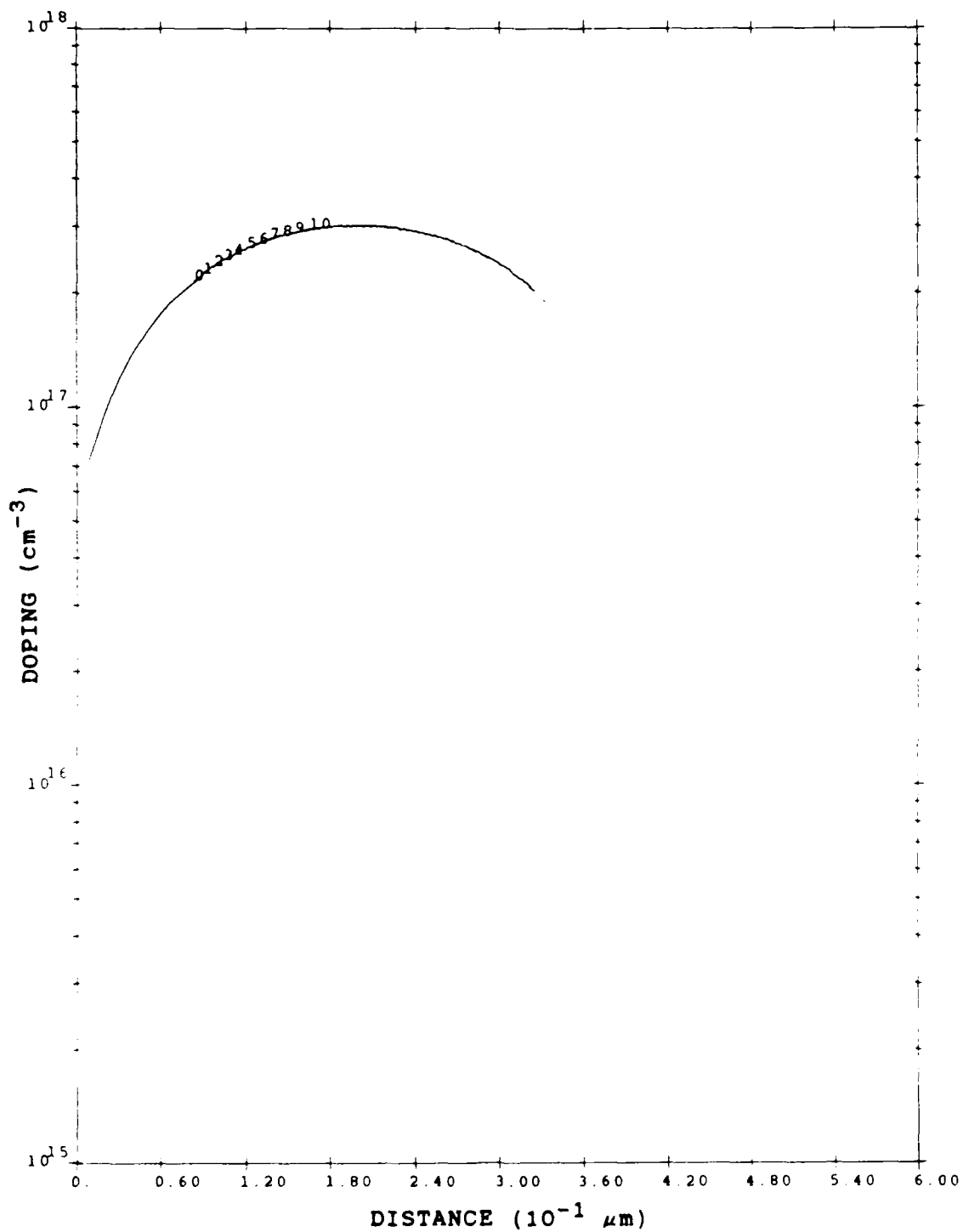Method for a Linear Profile

45

Figure 17.    Performance of the Voltage Second Derivative
             Method for the Parabolic Profile of Figure 18
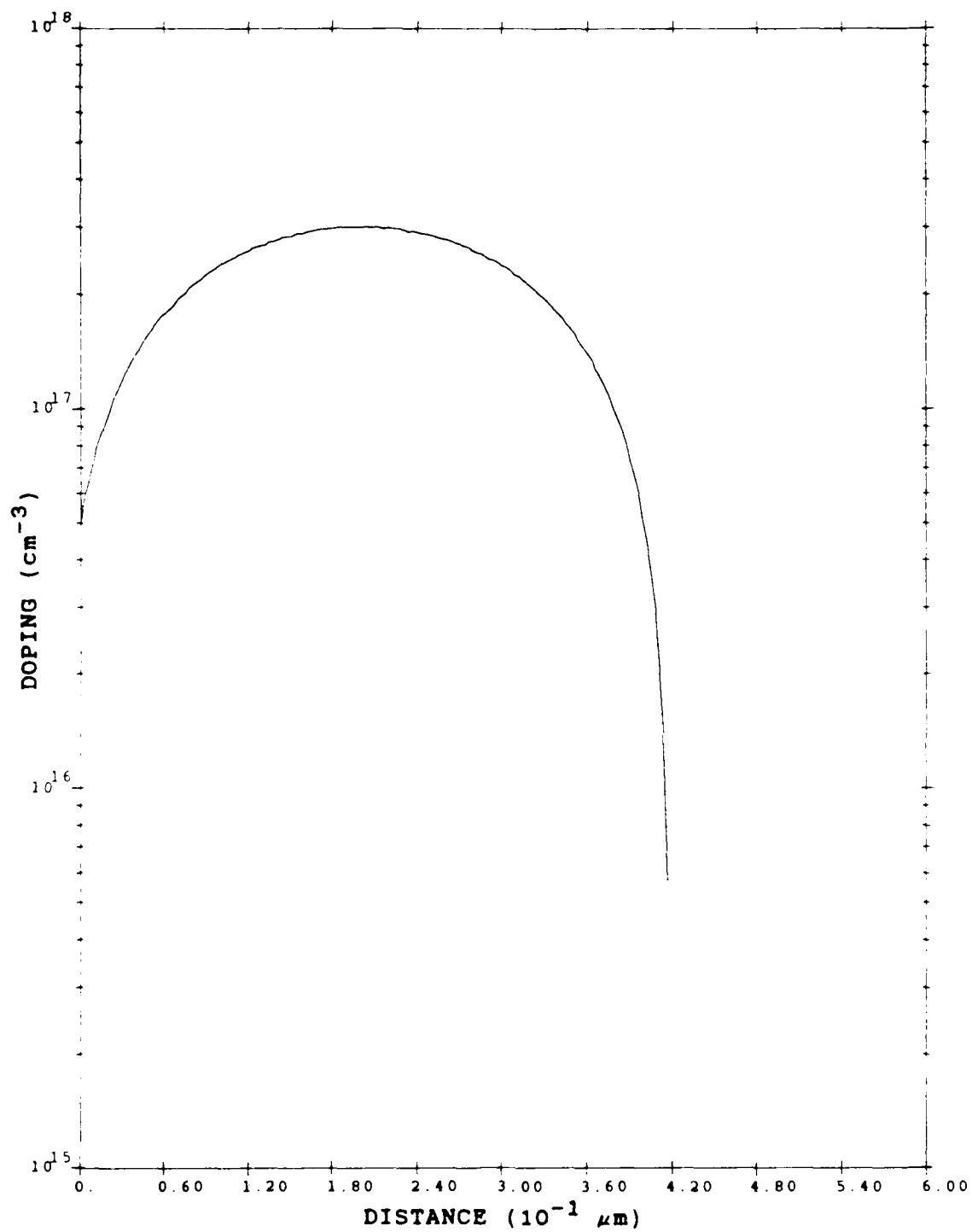
46

Figure 18.   A Parabolic Charge Carrier Profile
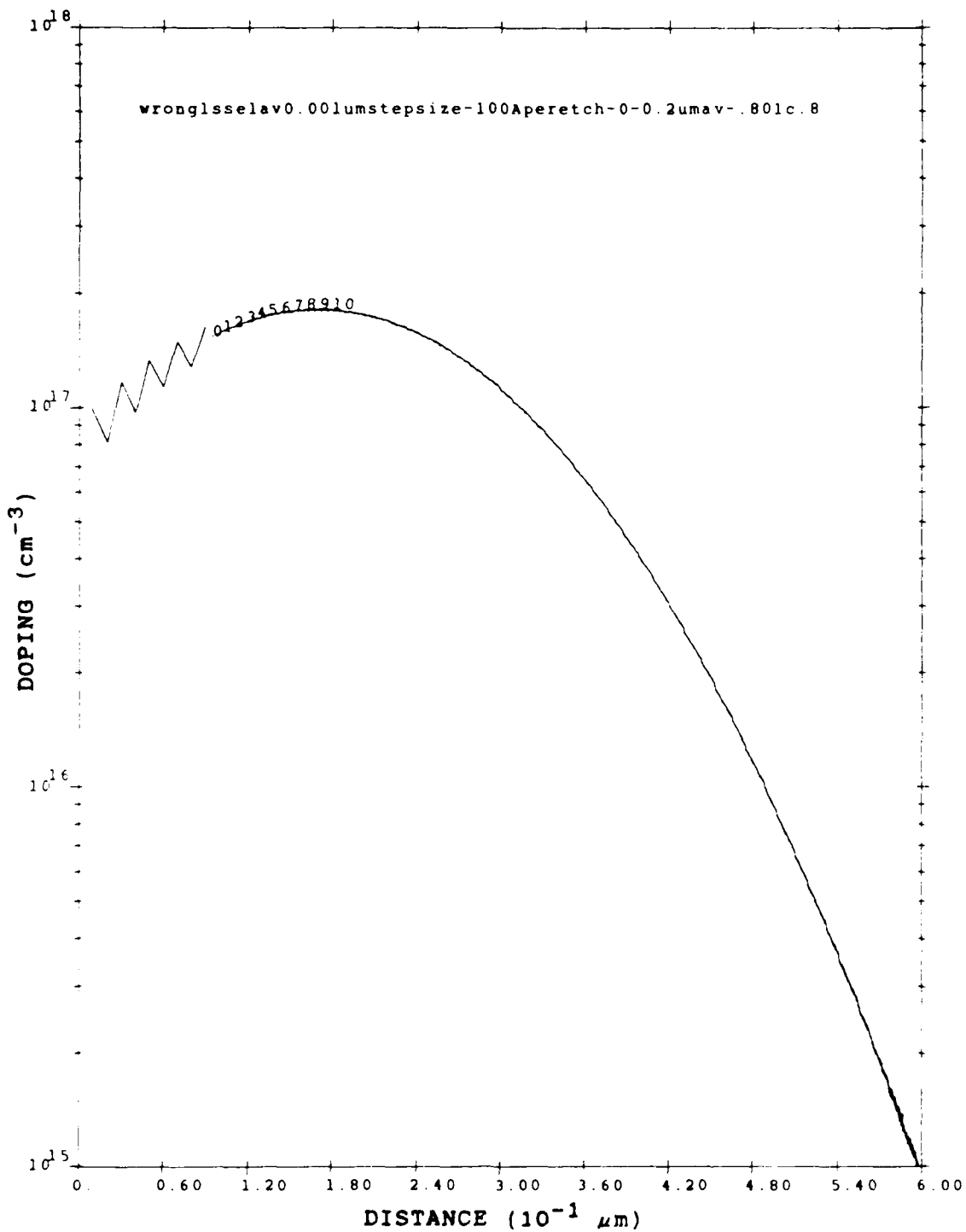
47

Figure 19.   Performance of the Voltage Second Derivative
             Method When the Voltages of Every Other Etch
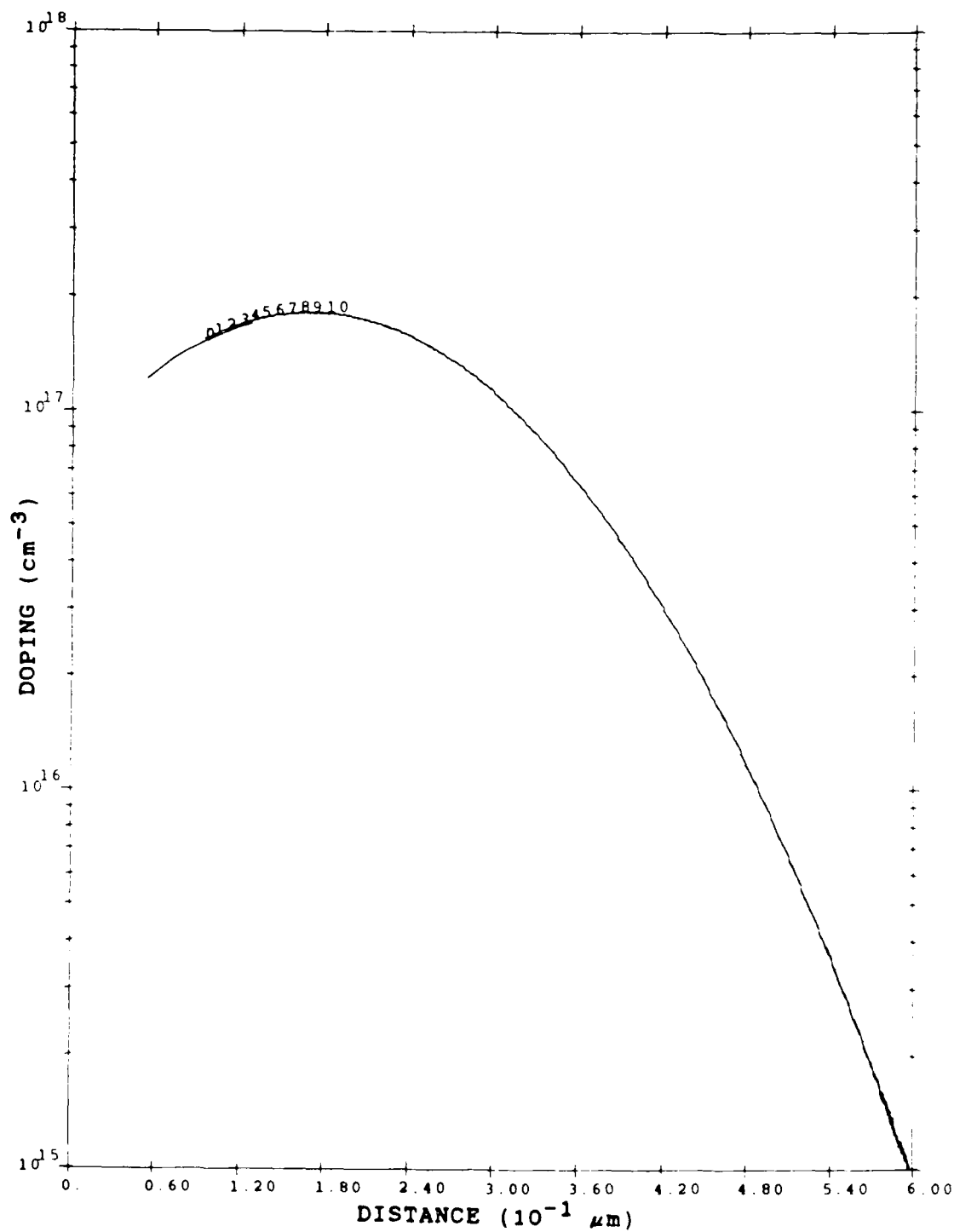             Curve are Offset by 1 mV

48

Figure 20. Performance of the Voltage First Derivative
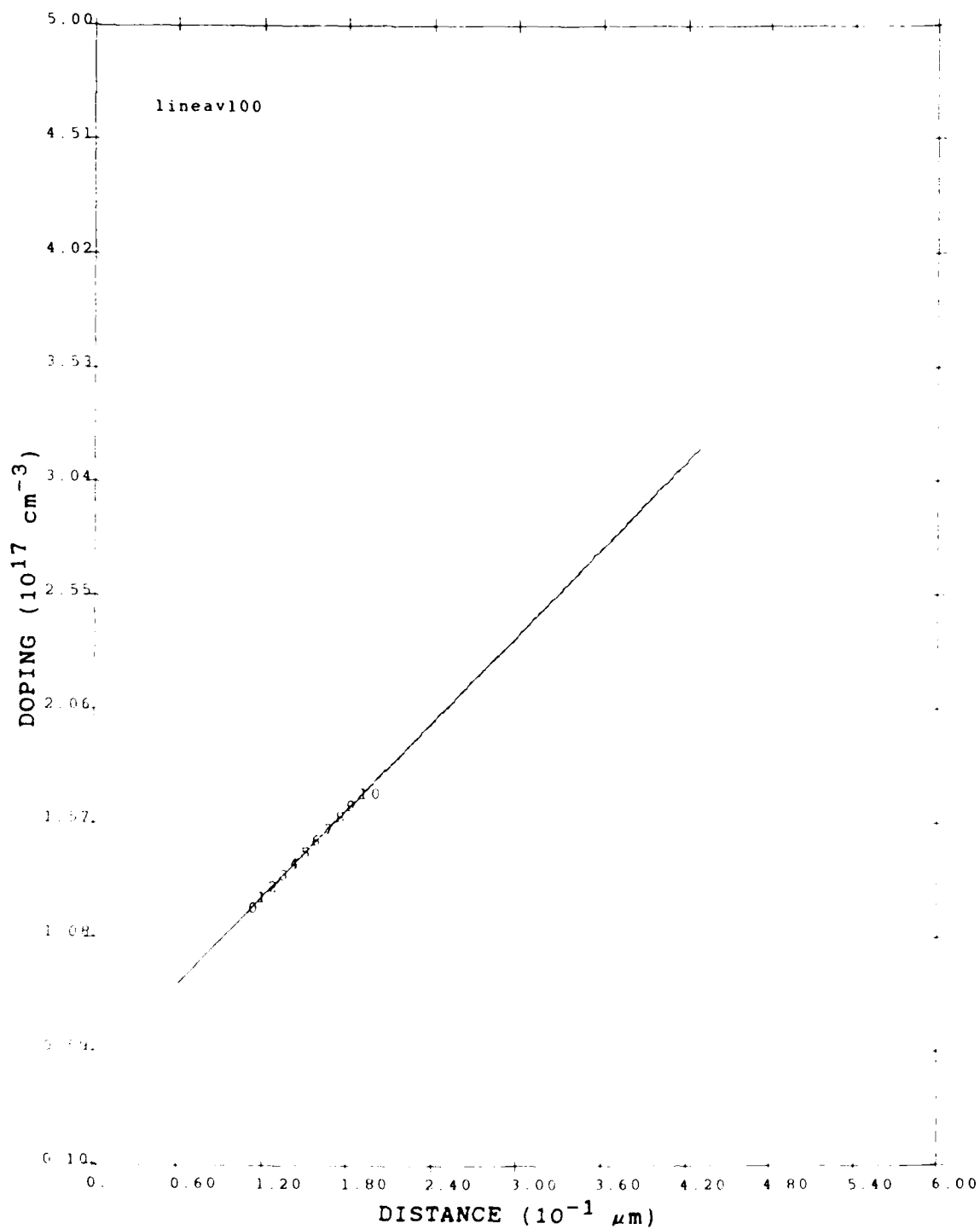Method for the LSS Profile of Figure 13

49

Figure 21.  Performance of the Voltage First Derivative
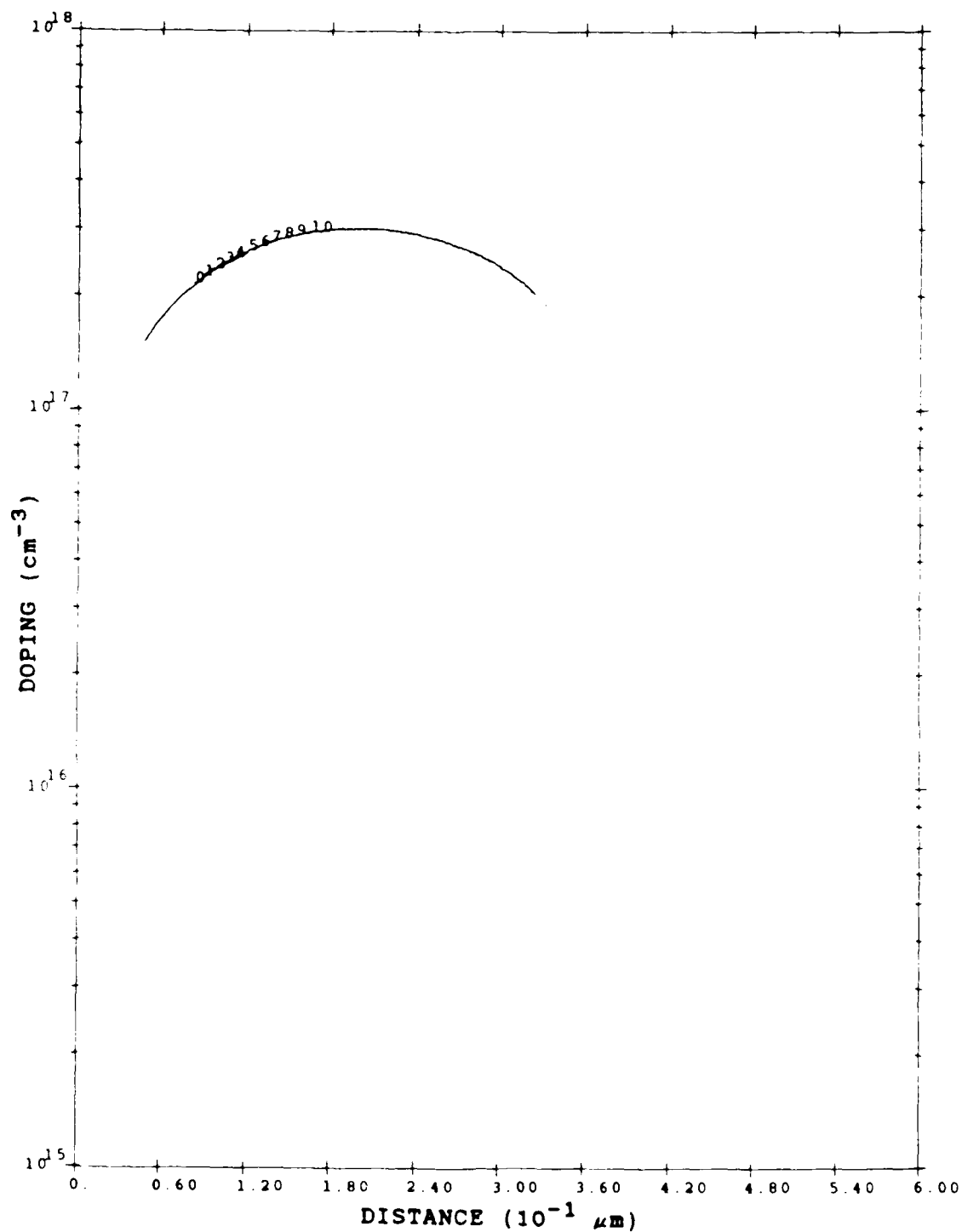Method for a Linear Profile

Figure 22.  Performance of the Voltage First Derivative
Method for the Parabolic Profile of Figure 18

51

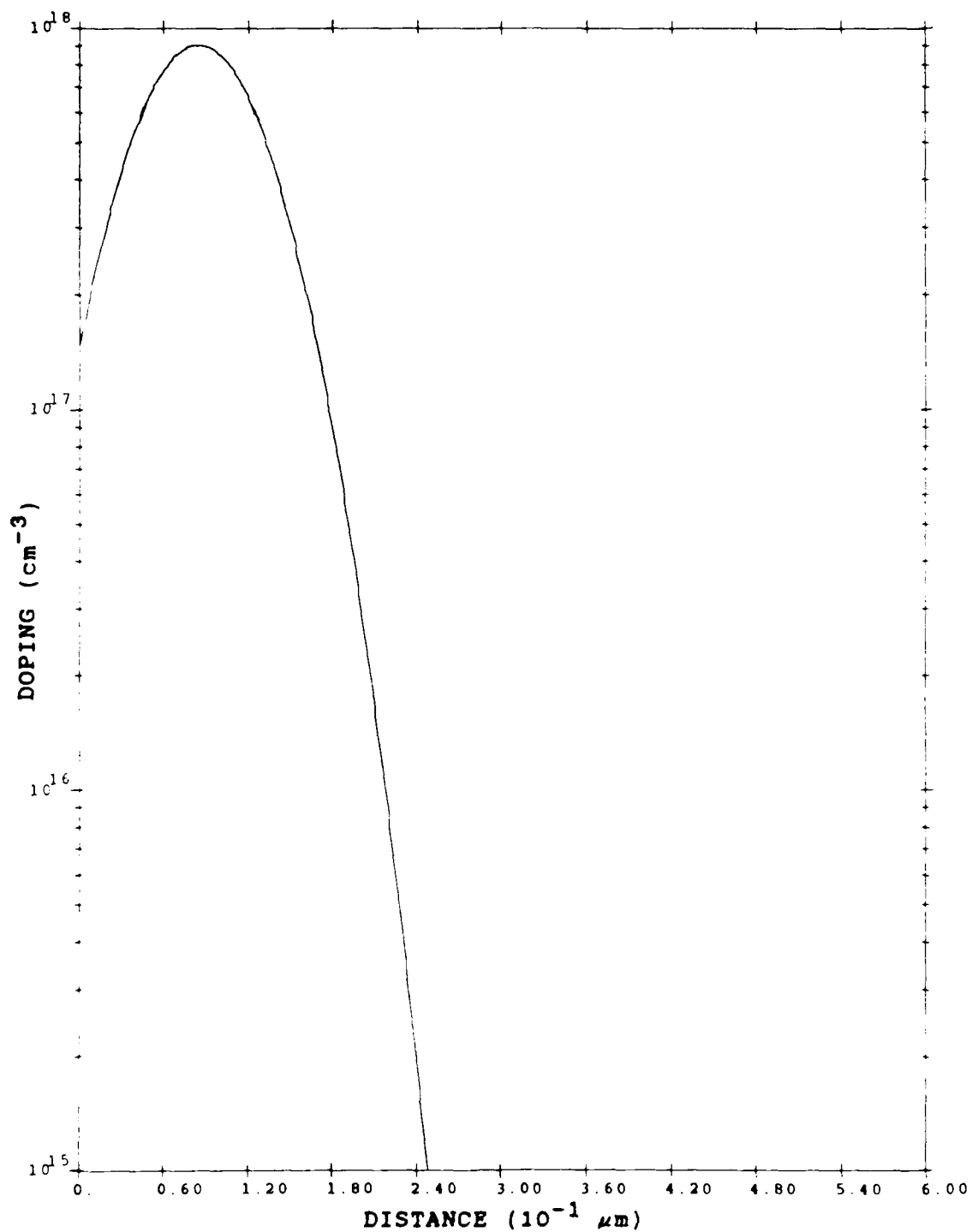Figure 23.   LSS Profile for Si-Implanted GaAs
             (Ion Dose: $1 \times 10^{13}$ cm$^{-2}$; Energy: 100 keV;
             Range: .085$\mu$m; Standard Deviation: .0442$\mu$m)

Figure 24. Performance of the Voltage First Derivative
Method for Sample A311

Figure 25.  Performance of the Voltage Second Derivative
Method for Sample A311 (Averaged Over the First
0.2 $\mu$m of Each C-V Profile)

54

Figure 26. Performance of the Voltage Second Derivative
Method for Sample A311 (Averaged Over the First
0.3 μm of Each C-V Profile)

55

Figure 27. Performance of the Voltage First Derivative
Method for Sample A312
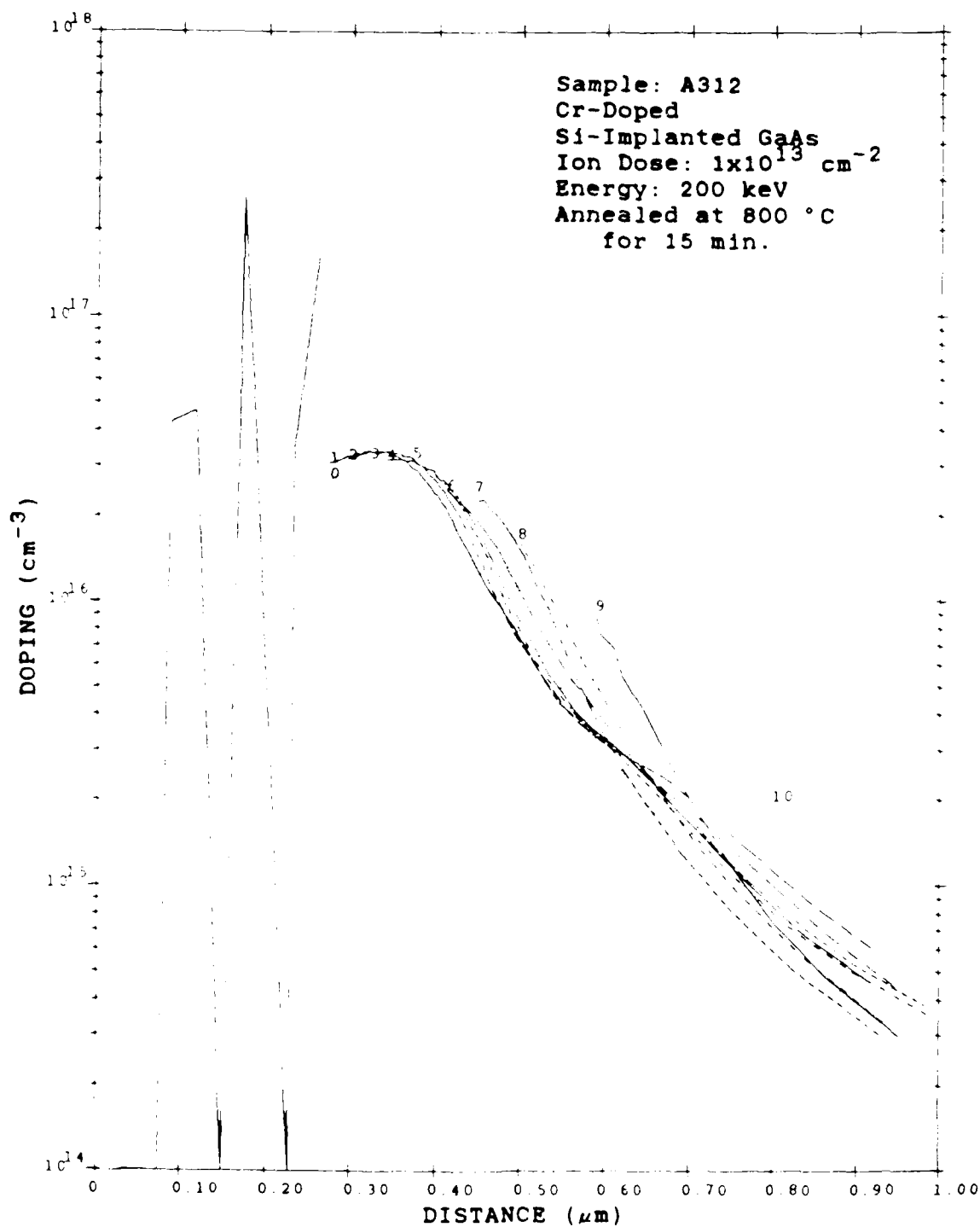
Figure 28. Performance of the Voltage Second Derivative Method for Sample A312 (Averaged Over the First 0.3 μm of Each C-V Profile)
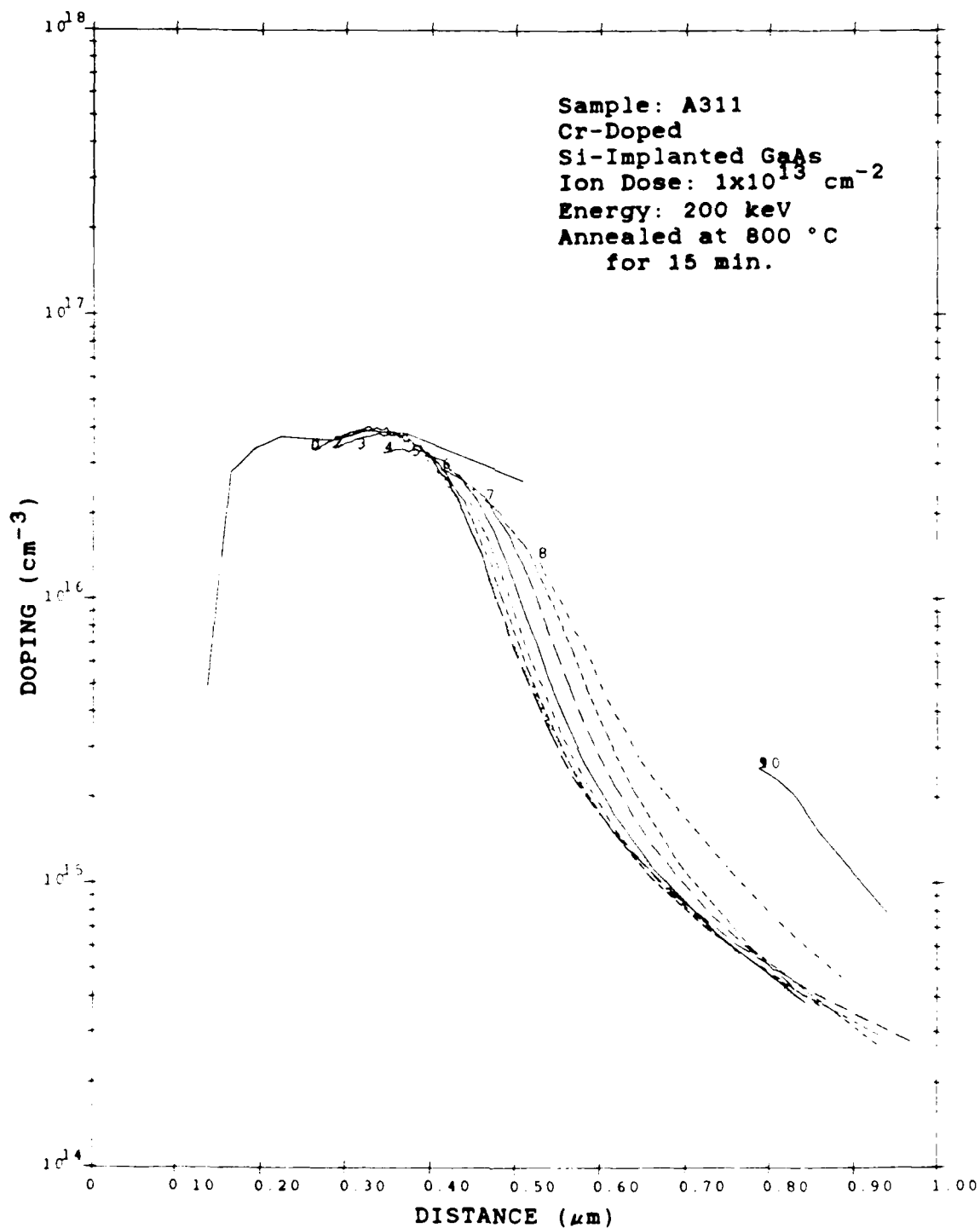
Figure 29.  Performance of the Voltage First Derivative
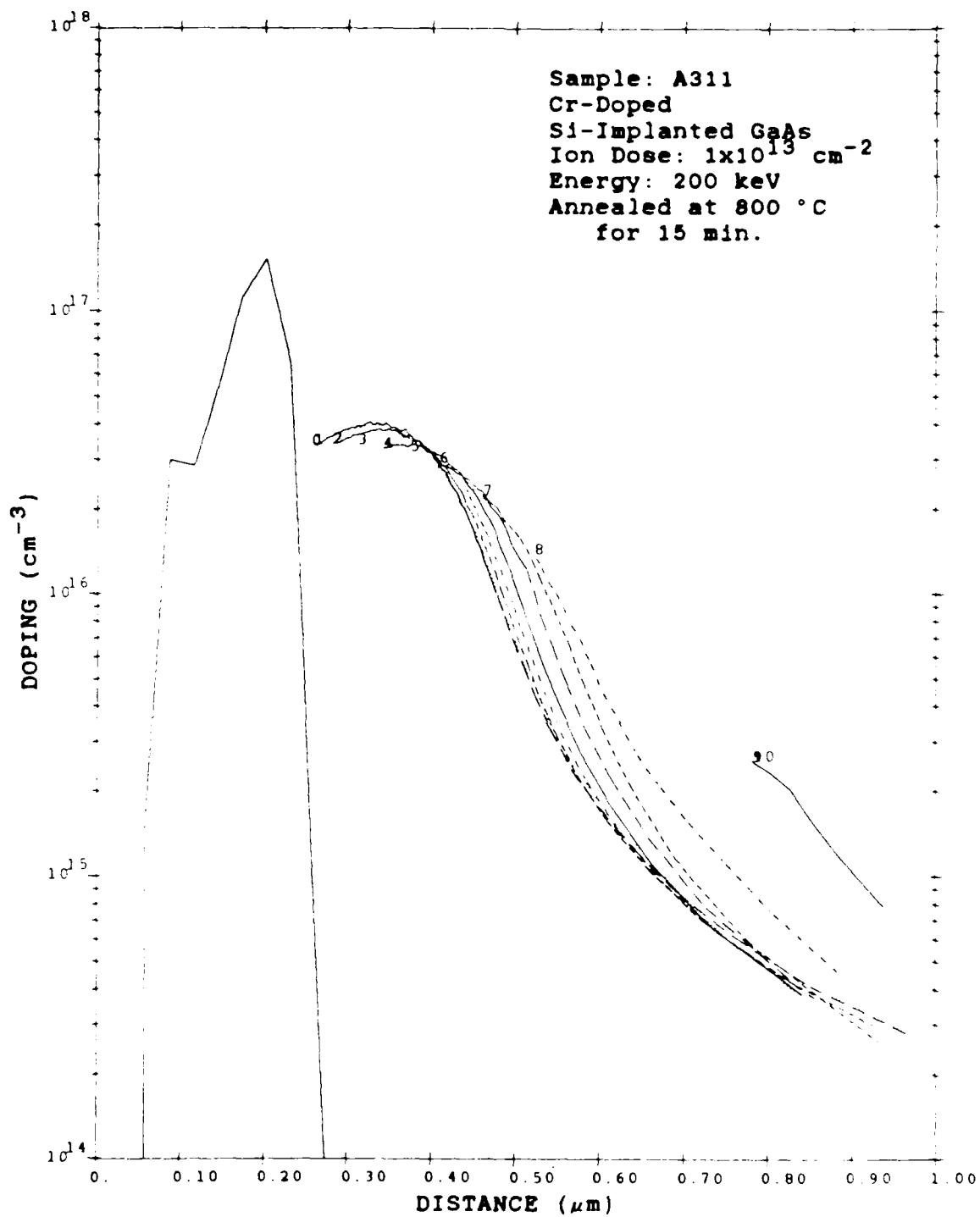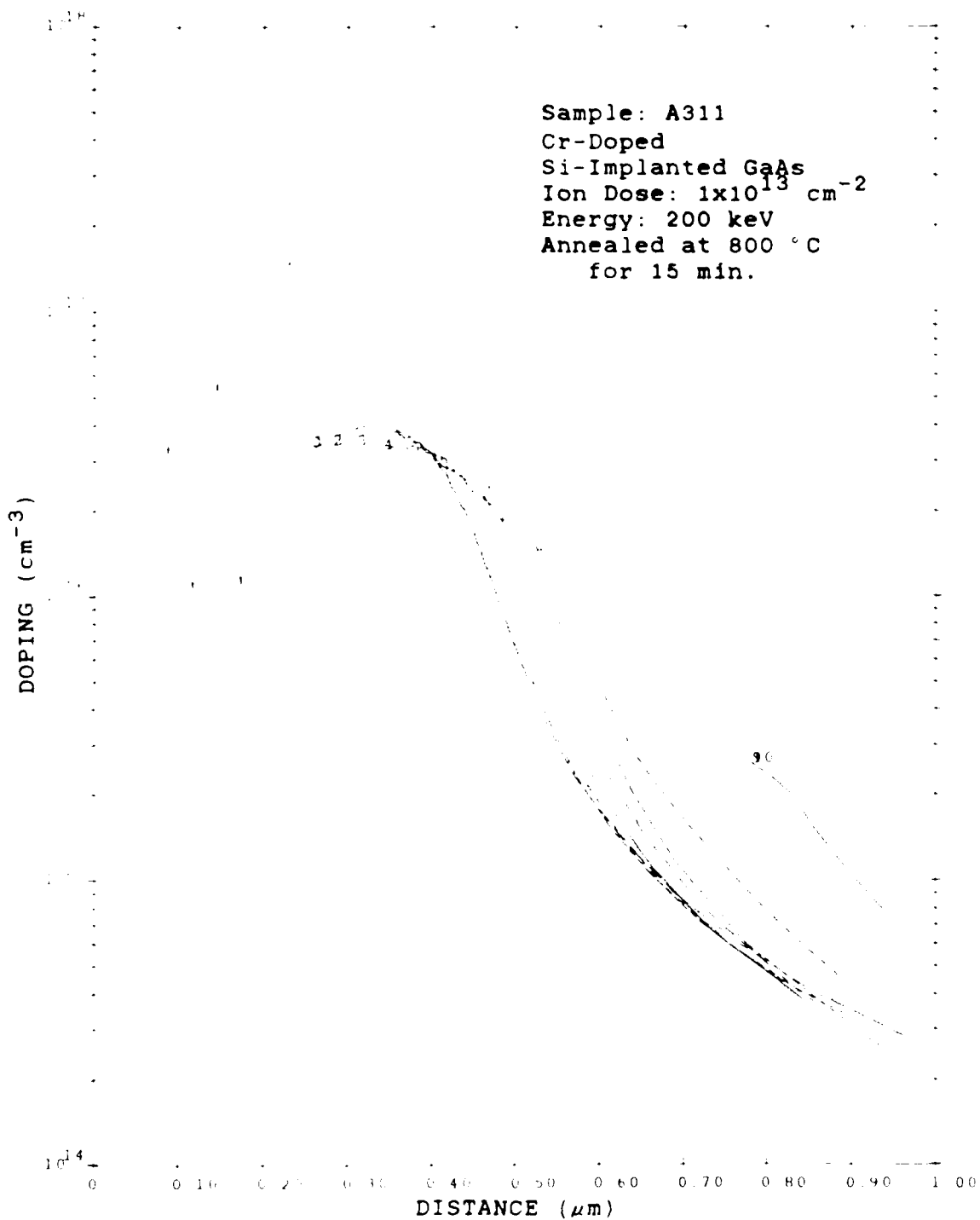            Method for Sample S021
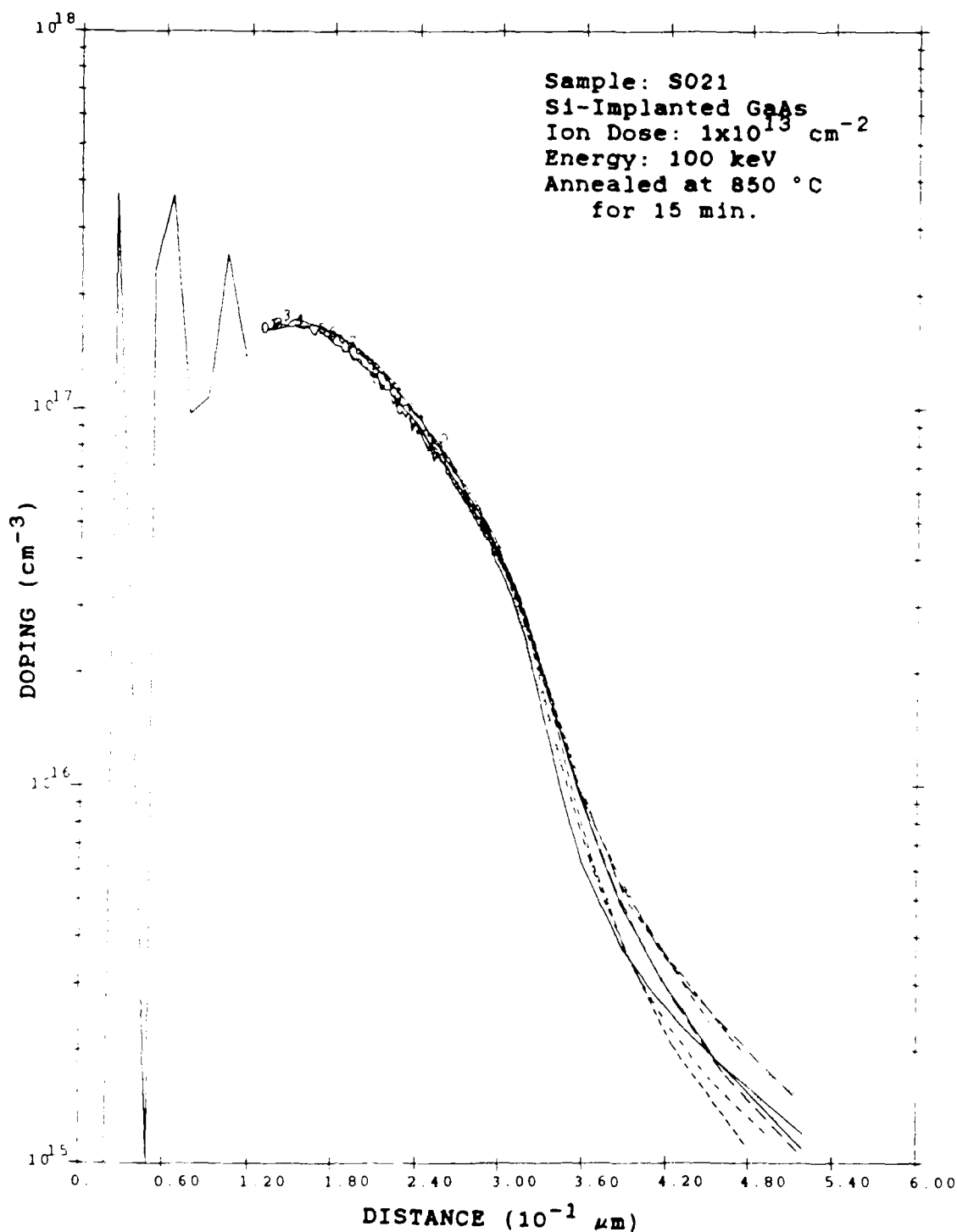
Figure 30. Performance of the Voltage Second Derivative Method for Sample S021 (Averaged Over the First 0.3μm of Each C-V Profile)

Figure 31. Performance of the Voltage Second Derivative Method for Sample S021 (Averaged Over a Range of 0.1 $\mu$m to 0.3 $\mu$m From the Start of Each C-V Profile)
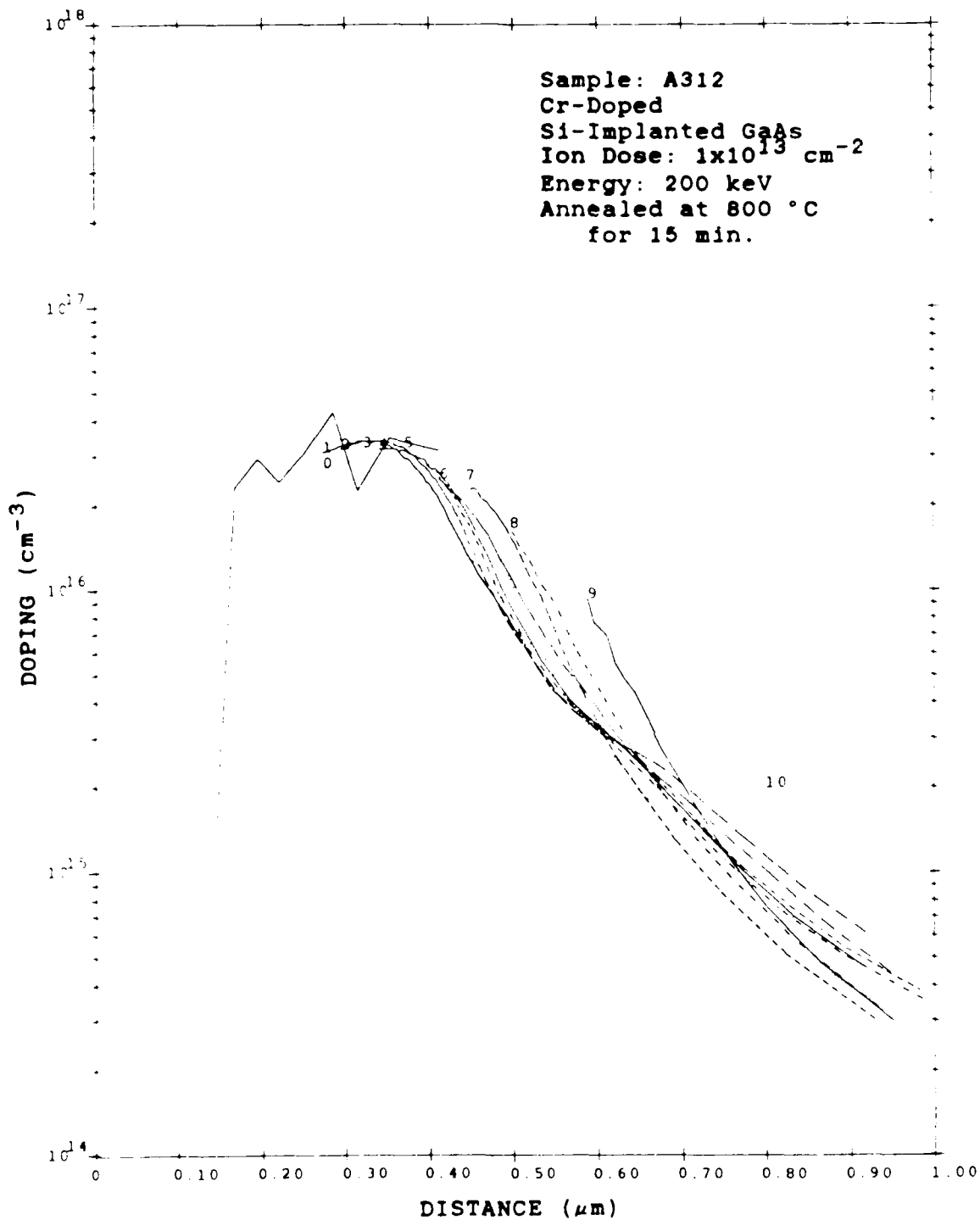
Figure 32. Performance of the Voltage First Derivative
Method for Sample S022

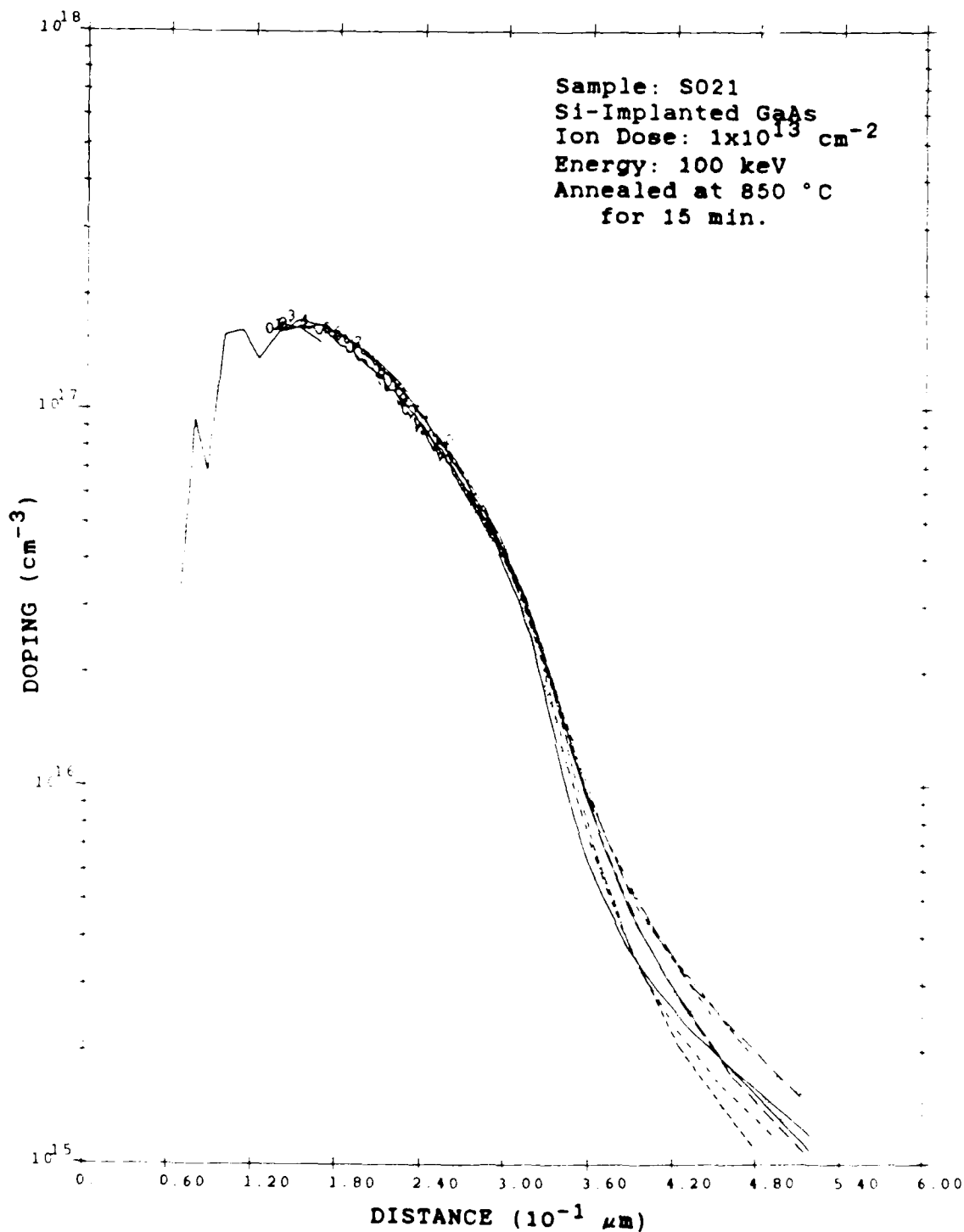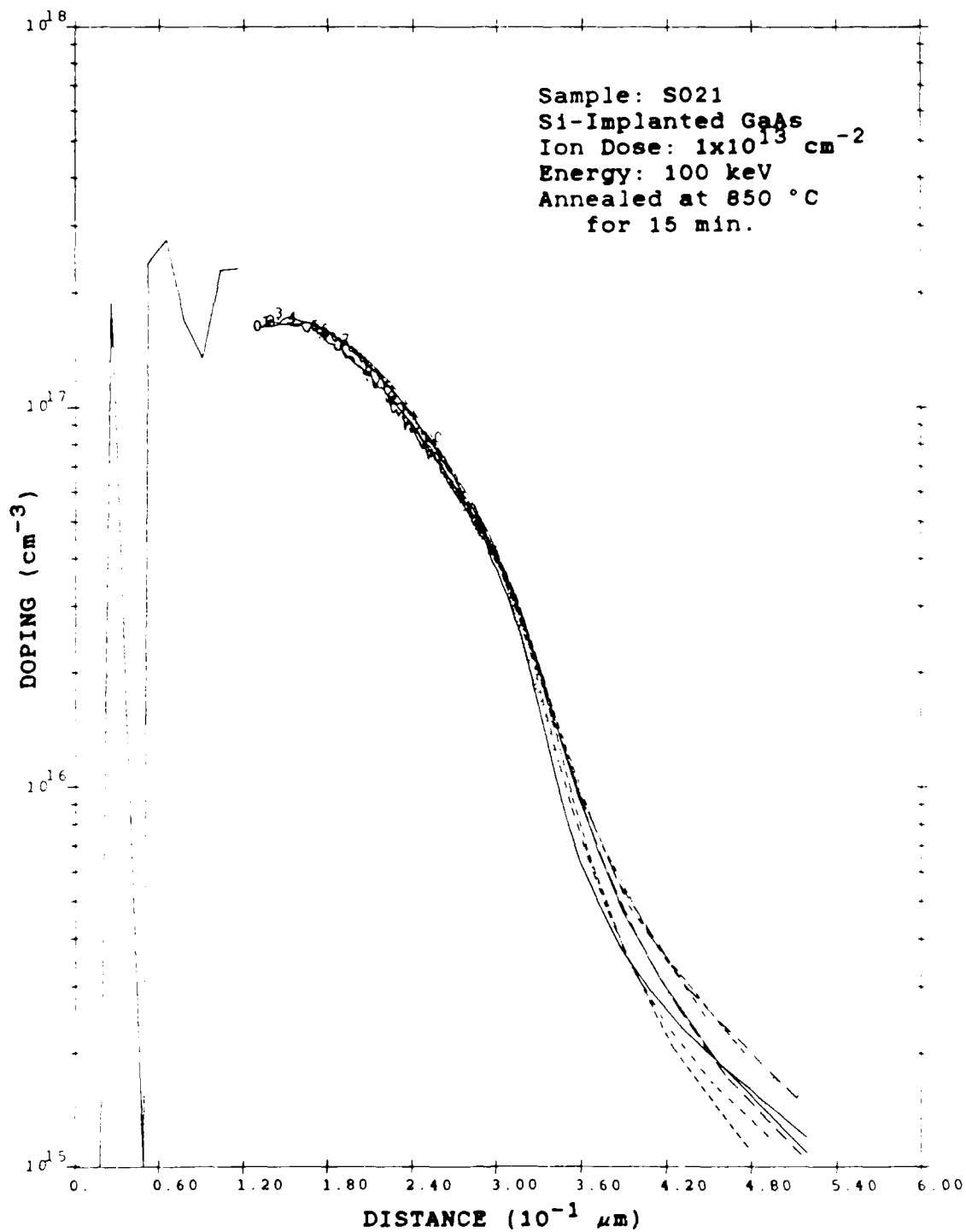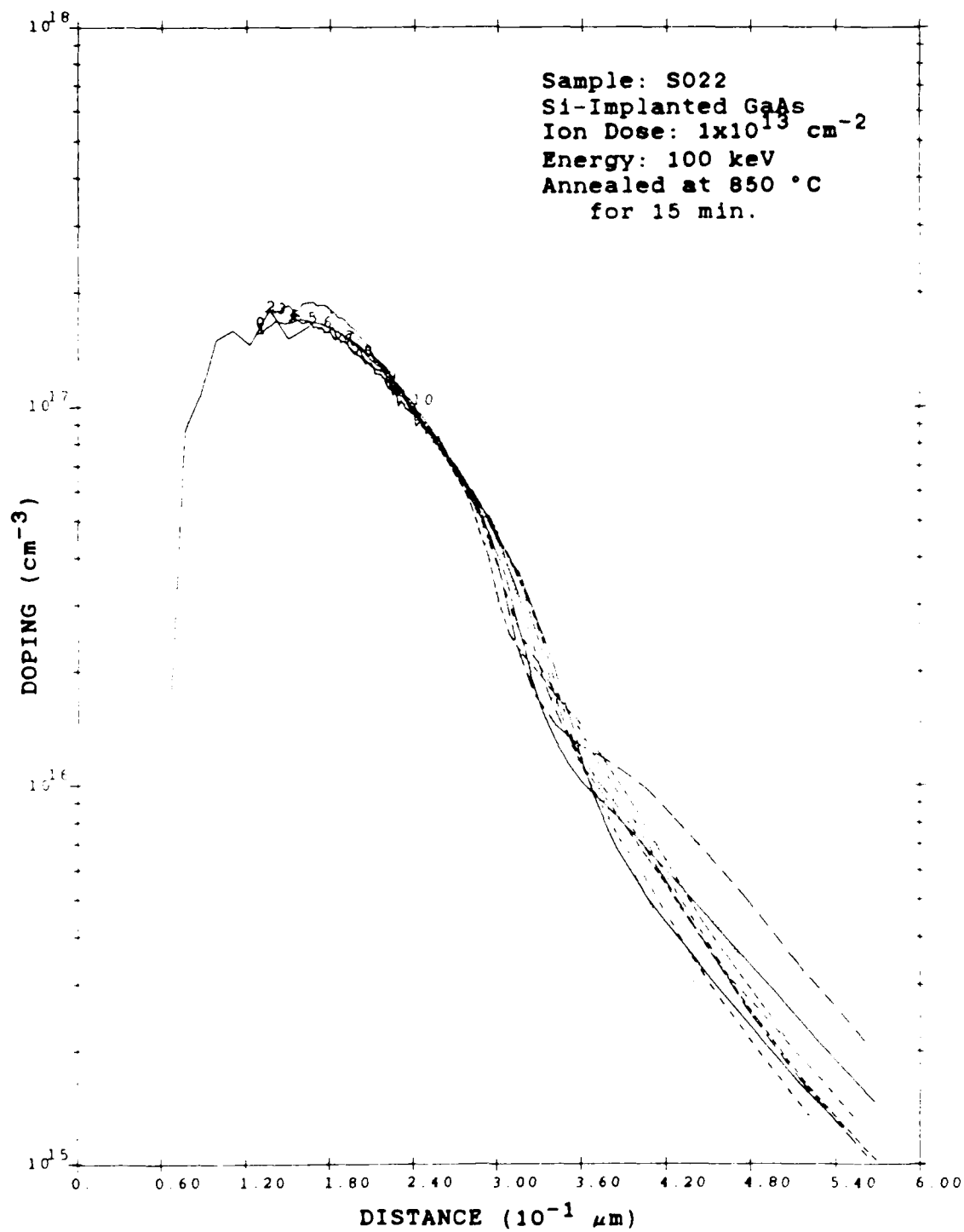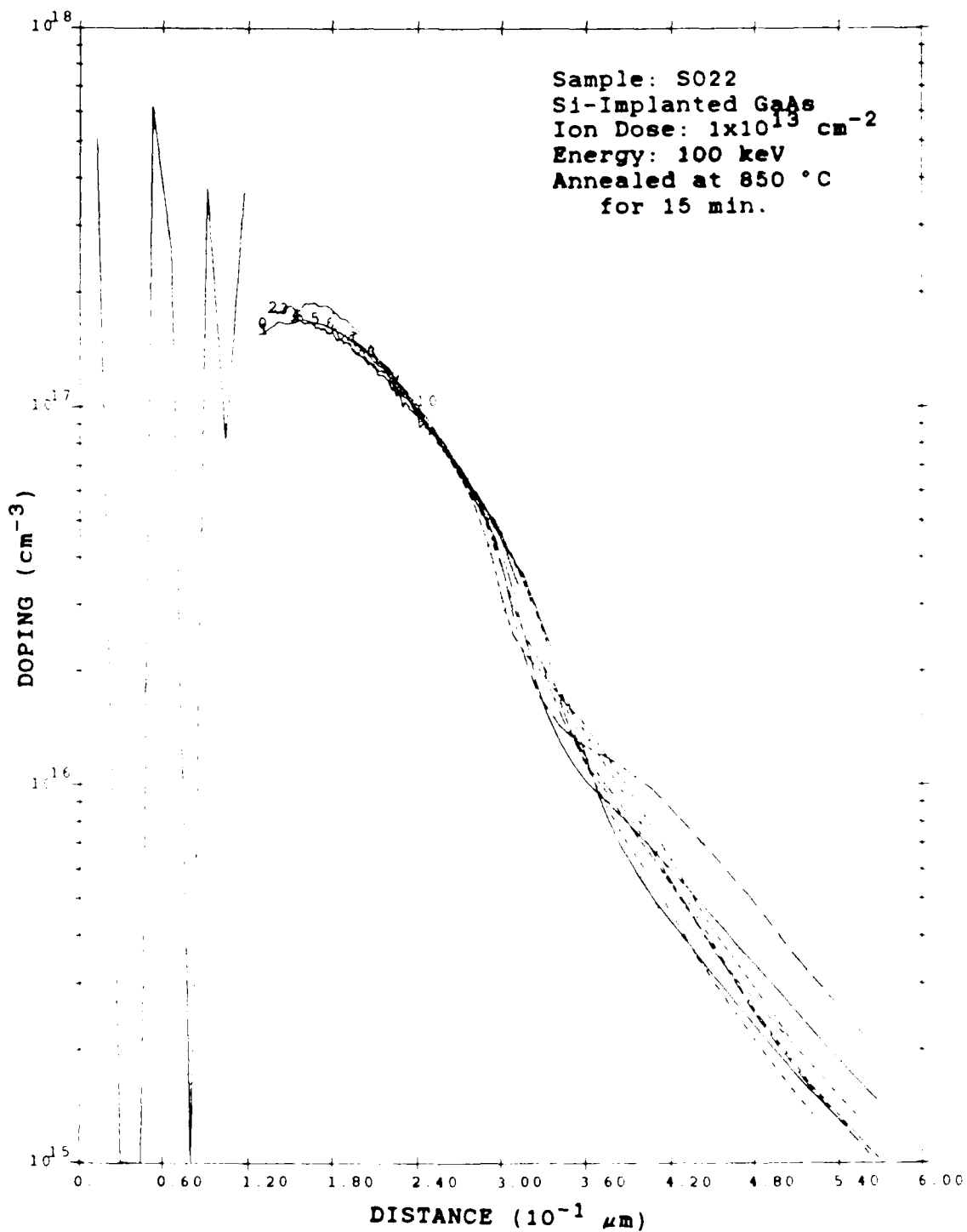**Figure 33.** Performance of the Voltage Second Derivative Method for Sample S022 (Averaged Over a Range of 0.03 to 0.13 μm from the Start of Each C-V Profile)

# VII. Conclusions and Recommendations

## Conclusions

Methods were developed for finding the charge carrier concentrations within the initial depletion region of n-type semiconductors. These methods combine the capacitance-voltage (C-V) technique with the etching of layers from the semiconductor surface. After each etch, the depletion region is made to end at the same location within the semiconductor. This location is used as a common reference and is arbitrarily chosen at a distance deep below the original unetched surface. For each etch depth, the voltage which extends the depletion region to the common reference distance is found. The voltage drop from an etch depth to the deeper common reference distance is the same as it would be if the semiconductor was not etched. This voltage drop is the sum of the applied voltage and the built-in potential. The built-in potential depends on the barrier potential at the semiconductor surface and the concentration at the common reference distance. Assuming the barrier potential is the same for each etch surface, the built-in potential is constant for each etch. Consequently, the applied bias voltage at each etch surface, can be treated as the potential at that etch depth. Then equations, such as Poisson's equation, can be used to find the carrier concentrations within the initial depletion

63

region. These methods were successfully applied to ideal computer generated C-V data as well as experimental C-V measurements of Si-implanted GaAs.

## Recommendations

Probably the main source of error in these methods is the fact that the depletion region ends gradually instead of abruptly. Wu et al. (22:319-329) showed how the shape of the depletion region changes with applied bias voltage for the regular C-V technique, and in a companion paper Klopfenstein and Wu (23:329-333) described computational methods for calculating the C-V measurements that would result from specified carrier distributions. These computational methods should be applied to check the accuracy of the methods developed in this thesis. The fact that the depletion region changes its shape should be less serious for the methods of this thesis than for the regular C-V technique, since a common reference distance is always used and each point in the depletion region should experience about the same potential regardless of whether material has been etched before it. If the common reference distance is far from the etch surfaces and the etch thicknesses are small, the basic shape of the depletion region should change little from one etch to the next. This is similar to an assumption for the regular C-V technique that the built-in potential changes little with increments in the applied bias voltage.

Another major source of error is oxidation of the semiconductor surface. The surface barrier height was assumed to remain constant for all the etch surfaces, but oxidation changes the barrier height. A change in the barrier height of 1 mV can very much change the concentration calculated. If the barrier height could be accurately measured for each etch surface, greater accuracy could be obtained and the methods could be simplified.

For greater accuracy, a much larger number of finer etches should be performed both within and outside the initial depletion region. Greater accuracy in the measurements of etch thicknesses, voltages, and capacitances would help. In this study, capacitances were measured to within 5, 4, and sometimes only 3 significant digits. The voltages may have been measured to within only 3 significant digits. The calculations were rather insensitive to inaccuracies in etch thicknesses, but the thicknesses were measured with an accuracy of about 10%.

## Bibliography

1.  Dearnaley, G. et al. Ion Implantation. Amsterdam: North-Holland Publishing Company, 1973.

2.  Morgan, D.V. et al. "Prospects for Ion Bombardment and Ion Implantation in GaAs and InP Device Fabrication," IEE Proceedings, 128: 109-130, August 1981.

3.  Stephens, K.G. and Sealy, B.J. "Use of ion implantation in future GaAs technology," Microelectronics, J.9: 13-18, 1978.

4.  Yeo, Y.K., et al. "Surface-depletion effect correction to nonuniform carrier distributions by Hall measurements," Journal of Applied Physics, 61(11): 5070-5075, June 1987.

5.  Gibbons, J.F. et al. "Projected Range Statistics: Semiconductors and Related Materials," Dowden, Hutchinson and Ross, Inc., 1975.

6.  Carter, G. and Grant, W.A. "Ion Implantation of Semiconductors," Chap. 3, Edward Arnold, Ltd., London, 1976.

7.  Chandra, A. et al. "Surface and Interface Depletion Corrections to Free Carrier Density Determinations by Hall Measurements," Solid State Electronics, 22, pp 645-650, December 1979.

8.  Many, A. et al. Semiconductor Surfaces. Amsterdam: North-Holland Publishing Company, 1965.

9.  Bardeen, J. "Surface States and Rectification at a Metal Semi-Conductor Contact," Physical Review, 71, pp 717-727, 1947.

10. McKelvey, J.P. Solid State and Semiconductor Physics. Malabar, Fla.: Robert & Krieger Publishing Co., 1966.

11. Shockley, W. "On the surface states associated with a periodic potential," Physical Review, 56, 317-323, August 1939.

12. Massies, J. et al. "Application of Molecular Beam Epitaxy to Study the Surface Properties of III-V Compounds," Proceedings of the 3rd International Conference on Solid Surfaces, pp 639-646, Vienna, 1977.

13. Henisch, H.K. *Rectifying Semiconductor Contacts*.
    Oxford: The Clarendon Press, 1957.

14. Schottky, W. "Verinfachte und Erweiterte Theorie der
    Randschichtgleichricter," *Zeitchrift fur Physik*, 118,
    pp 539-592, September 1942.

15. Copeland, J.A. "A Technique for Directly Plotting the
    Inverse Doping Profile of Semiconductor Wafers," *IEEE
    Transactions on Electron Devices*, ED 16, No 5,
    pp 445-449, May 1969.

16. Miller, L. "A Feedback Method for Investigating Carrier
    Distributions in Semiconductors," *IEEE Transactions on
    Electron Devices*, ED 19, No 10, pp 1103-1198, October
    1982.

17. Nakhamanson, R.S. "A Technique for Directly Plotting
    the Doping Profile of Semiconductor Wafers ('8-Shaped
    Way')," *Solid State Electronics*, 19, pp 84-89, 1976.

18. Sze, S.M. *Physics of Semiconductor Devices*, (2nd Ed.).
    Murray Hill, New Jersey: John Wiley & Sons, 1981.

19. Kim, Y.Y. *Electrical Properties of Silicon-Implanted
    GaAs*. MS Thesis. PH-82D-17. School of Engineering, Air
    Force Institute of Technology (AU), Wright-Patterson
    AFB, OH, December 1982.

20. Giacoletto, L. "Junction Capacitance and Related
    Characteristics Using Graded Imputity Semiconductors,"
    *IRE Transactions on Electron Devices*, ED 4, pp 207-215,
    July 1957.

21. Norwood, H.M. et al. "Voltage Variable Capacitor
    Tuning: A Review," *Proceedings of the IEEE*, Vol 56,
    No 5, pp 788-798, May 1968.

22. Wu, C.P. et al. "Limitations of the CV Technique for
    Ion-Implanted Profiles," *IEEE Transactions on Electron
    Devices*, ED 22, No 6, pp 319-329, June 1975.

23. Klopfenstein, R.W. and Wu, C.P. "Computer Solution of
    One-Dimensional Poisson's Equation," *IEEE Transactions
    on Electron Devices*, ED 22, No 6, pp 329-333, June
    1975.

## VITA

Gordon H. Gainer, Jr. was born on 16 January 1960 in Newark, Ohio. He graduated from Heath High School in 1978 and then attended Ohio State University, from which he received a Bachelor of Science in Engineering Physics. He received a commission in the USAF through the Officer Training School. His first assignment was to the Aero Propulsion Laboratory, with a subsequent assignment to the Air Force Institute of Technology, both at Wright-Patterson AFB, Ohio. His next assignment in 1988 was to the Technical Operations Division of the Air Force Technical Applications Center at McClellan AFB, California.
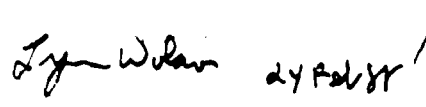
<div style="text-align: center">

Permanent Address: 6300 Dundee Dr.
North Highlands CA   95660

</div>

# REPORT DOCUMENTATION PAGE

Form Approved
OMB No. 0704-0188

| 1a REPORT SECURITY CLASSIFICATION | 1b RESTRICTIVE MARKINGS |
|---|---|
| UNCLASSIFIED | |

| 2a SECURITY CLASSIFICATION AUTHORITY | 3 DISTRIBUTION/AVAILABILITY OF REPORT |
|---|---|
| 2b DECLASSIFICATION/DOWNGRADING SCHEDULE | Approved for public release; distribution unlimited. |

| 4 PERFORMING ORGANIZATION REPORT NUMBER(S) | 5 MONITORING ORGANIZATION REPORT NUMBER(S) |
|---|---|
| AFIT/GEP/ENP/87D-8 | |

| 6a NAME OF PERFORMING ORGANIZATION | 6b OFFICE SYMBOL (If applicable) | 7a NAME OF MONITORING ORGANIZATION |
|---|---|---|
| School of Engineering | AFIT/ENP | |

| 6c ADDRESS (City, State, and ZIP Code) | 7b ADDRESS (City, State, and ZIP Code) |
|---|---|
| Air Force Institute of Technology (AU) Wright-Patterson AFB, Ohio 45433-6583 | |

| 8a NAME OF FUNDING/SPONSORING ORGANIZATION | 8b OFFICE SYMBOL (If applicable) | 9 PROCUREMENT INSTRUMENT IDENTIFICATION NUMBER |
|---|---|---|
| | | |

| 8c ADDRESS (City, State, and ZIP Code) | 10 SOURCE OF FUNDING NUMBERS | | | |
|---|---|---|---|---|
| | PROGRAM ELEMENT NO | PROJECT NO | TASK NO | WORK UNIT ACCESSION NO |
| | | | | |

11 TITLE (Include Security Classification)
CALCULATING DEPLETION REGION CARRIER CONCENTRATIONS WITH CAPACITANCE-VOLTAGE MEASUREMENTS AND ETCHING (UNCLASSIFIED)

12 PERSONAL AUTHOR(S)
Gordon H. Gainer, Jr., Capt, USAF

| 13a TYPE OF REPORT | 13b TIME COVERED | | 14 DATE OF REPORT (Year, Month, Day) | 15 PAGE COUNT |
|---|---|---|---|---|
| MS Thesis | FROM ___ TO ___ | | 1987 December | 79 |

16 SUPPLEMENTARY NOTATION

| 17 | COSATI CODES | | 18 SUBJECT TERMS (Continue on reverse if necessary and identify by block number) |
|---|---|---|---|
| FIELD | GROUP | SUB-GROUP | Surface Depletion, Depletion Region, Carrier Concentration Profiles, Ion Implantation, CAPACITANCE-VOLTAGE TECHNIQUE, C-V TECHNIQUE |
| 20 | 12 | | |

19 ABSTRACT (Continue on reverse if necessary and identify by block number)

Title: CALCULATING DEPLETION REGION CARRIER CONCENTRATIONS WITH CAPACITANCE-VOLTAGE MEASUREMENTS AND ETCHING

Thesis Chairman: Yung Kee Yeo, Ph.D.
Professor of Physics

| 20 DISTRIBUTION/AVAILABILITY OF ABSTRACT | 21 ABSTRACT SECURITY CLASSIFICATION |
|---|---|
| ☒ UNCLASSIFIED/UNLIMITED ☐ SAME AS RPT ☐ DTIC USERS | UNCLASSIFIED |

| 22a NAME OF RESPONSIBLE INDIVIDUAL | 22b TELEPHONE (Include Area Code) | 22c OFFICE SYMBOL |
|---|---|---|
| Yung Kee Yeo, Ph.D. | 513-255-4498 | AFIT/ENP |

**DD Form 1473, JUN 86**       Previous editions are obsolete       SECURITY CLASSIFICATION OF THIS PAGE

Methods were developed for finding the charge carrier concentrations within the initial depletion region of n-type semiconductors. These methods combine the capacitance-voltage (C-V) technique with the etching of layers from the semiconductor surface. After each etch, the depletion region is made to end at the same location within the semiconductor. This location is used as a common reference and is arbitrarily chosen at a distance deep below the original unetched surface. For each etch depth, the voltage which extends the depletion region to the common reference distance is found. The voltage drop from an etch depth to the deeper common reference distance is the same as it would be if the semiconductor was not etched. This voltage drop is the sum of the applied voltage and the built-in potential. The built-in potential depends on the barrier potential at the semiconductor surface and the concentration at the common reference distance. Assuming the barrier potential is the same for each etch surface, the built-in potential is constant for each etch. Consequently, the applied bias voltage at each etch surface, can be treated as the potential at that etch depth. Then equations, such as Poisson's equation, can be used to find the carrier concentrations within the initial depletion region. These methods were successfully applied to ideal computer generated C-V data as well as experimental C-V measurements of Si-implanted GaAs.

# END

## DATE

FILMED

APRIL

1988

DTIC